AGU100 ADVANCING EARTH AND SPACE SCIENCE

Geochemistry, Geophysics, Geosystems

RESEARCH ARTICLE
10.1002/2017GC007344

Magnetism at Depth: A View from an Ancient Continental Subduction and Collision Zone

Suzanne A. McEnroe[1], Peter Robinson[2], Nathan Church[1], and Michael Purucker[3]

[1]Institute for Geoscience and Petroleum, Norwegian University of Science and Technology, Trondheim, Norway, [2]Geological Survey of Norway, Trondheim, Norway, [3]NASA—Goddard Space Flight Center, Greenbelt, MD, USA

Key Points:
- Nature and magnetic properties of oxides in high-pressure and ultrahigh pressure rocks in the lower crust, and upper mantle
- Effects of subduction, exhumation and failure to reach equilibrium mineral assemblages on the magnetism of continental crust
- Seeking the sources of long-wavelength magnetic anomalies measured by satellite surveys

Supporting Information:
- Supporting Information S1
- Table S1

Correspondence to:
S. A. McEnroe,
Suzanne.mcenroe@ntnu.no

Citation:
McEnroe, S. A., Robinson, P., Church, N., & Purucker, M. (2018). Magnetism at depth: A view from an ancient continental subduction and collision zone. *Geochemistry, Geophysics, Geosystems*, *19*. https://doi.org/10.1002/2017GC007344

Received 17 NOV 2017
Accepted 4 MAR 2018
Accepted article online 12 MAR 2018

Abstract Recent sophisticated global data compilations and magnetic surveys have been used to investigate the nature of magnetization in the lower crust and upper mantle. Two approaches to constraining magnetizations are developed, providing minimum (0.01 SI) and maximum (0.04 SI) susceptibility estimates, given some assumed thickness (15+ km here). These values are higher than are found in many continental rocks. Are there rocks deeper in the crust or upper mantle that are more magnetic than expected, or are the model assumptions incomplete? What is the magnetic behavior of deep-crustal and upper mantle rocks, when slightly cooler than the Curie or Néel temperatures of their magnetic minerals, after being exhumed from locations of high-grade metamorphism at greater depth? Different sets of equilibrium metamorphic minerals can be considered that would form under different conditions. Results on 1,501 samples from the Western Gneiss Region (WGR) Norway, mainly from mafic and ultramafic bodies subducted to depths of 60–200 km and temperatures of 750 up to 950°C at the very highest pressures, show that rocks did not fully equilibrate to the dominant metamorphic-facies conditions. There is a large variation in petrophysical properties, oxide minerals, and mineral assemblages in WGR samples, though they cannot explain the broad high-amplitude (deep-seated) anomalies measured in this region. The presence of magnetite, and exsolved titanohematite and hemoilmenite in samples, shows those magnetic phases are preserved even at eclogite-facies conditions, in part because complete eclogite-facies equilibrium was rarely achieved.

Plain Language Summary From the surface of the Earth down to the depth of what we call the Curie/Neel temperature, the crust can act as a magnetic tape recorder. The magnetic history is recorded and a memory kept for thousands (in essence a present-day magnetic memory) to an ancient memory that can be more than a billion years old. The preservation of this memory depends on temperature and pressure conditions, and oxide mineralogy. Today we read this memory from satellite data, or explore Earth's crust from high-resolution aeromagnetic surveys. It is challenging to understand the nature of the magnetic signature of the Earth provided by deep-seated rocks, because there are few areas on Earth with exceptional exposures of rocks, which have been exhumed from great depths. Here we explore the magnetic properties of rocks subducted to high-pressure and ultrahigh-pressure conditions in the Western Gneiss Region of Norway, famous for the eclogites found there. These show large variations in petrophysical properties, oxide minerals, and mineral assemblages, and provide new insights into the potential magnetic behavior of Earth's lithosphere at depth. These results are primary data that allow us to constrain and test current interpretations of the structure of the crust made from satellite surveys.

1. Introduction

The contribution to lithospheric magnetization from deep-crustal rocks remains enigmatic. Current models use crustal thicknesses derived from seismic and thermal studies, and then attempt to fit satellite magnetic data using a magnetic response dominantly in the direction of the present-day field. Based on these models, and constraints imposed on the magnetization, irrespective of its direction, the magnetic signature of the crust here is best fitted using susceptibility values of between 0.01 and 0.04 (SI) and/or magnetizations in the range from 0.4 to 1.6 A/m (Parker, 2003; Thébault et al., 2010). These susceptibility values are higher than is commonly found in many continental rocks in Scandinavia. For comparison, a Geological Survey of

Finland Report (Airo & Säävuori, 2013) based on >130,000 samples found that nearly 75% of the susceptibility values are paramagnetic, defined as volume susceptibilities (k) < 0.002 (SI). In the rocks above this value remanent magnetization accounts for >50% of the total magnetization in many rock types and is "especially significant for metamorphic rocks." Given the large number of surface samples that are in the paramagnetic range, it remains an open question whether there are rocks at depth in the crust that are more magnetic than expected, if parts of the mantle could contribute, or if assumptions in the model are incorrect.

The magnetic response of deep-crustal rocks is strongly controlled by (1) the abundance of magnetic minerals and their properties, in turn controlled by mineral reactions that took place during their entire history, involving changing P-T conditions and availability of fluids, and (2) the thermal structure of the crust.

Oceanic subduction zones have been proposed as areas of enhanced magnetic signal (Blakely et al., 2005) due to production of magnetite through serpentinization, however, metamorphism can also result in deserpentinization, where the secondary magnetite is reacted out. Contributions from serpentized mantle rocks would depend on the compositions of olivine and pyroxene, fluid availability, temperature (T), and pressure (P) regimes capable of producing magnetite, and the geotherm in localities of serpentinized mantle. Higher-grade metamorphism of mafic rocks to eclogite in such zones, where Fe^{2+} is sequestered into garnet, can cause major changes in magnetic mineralogy.

Another source of magnetism deep in the crust is from subduction of continental crust, where material is recycled into the mantle. Under such conditions and with adequate fluid, mafic rocks can convert to garnet and pyroxene, in process destroying all Fe-Ti oxides, leaving only a rutile-bearing paramagnetic residuum. In the Western Gneiss Region of Norway (WGR), there are large exposed areas of continental crust (28,000 km^2) that have been subducted to >60 km depth in the Lower Devonian Scandian continental collision, where they experienced eclogite-facies conditions, and then were exhumed back to near-surface conditions, further modified in that journey, depending on particular retrograde conditions. Few magnetic studies exist on such high-pressure rocks and their retrograded equivalents. The WGR offers an exceptional area for examining the effects of subduction and exhumation processes on magnetic properties of mafic continental crust and associated mantle peridotites.

Here we present the magnetic properties and oxides of 1,501 samples, mainly from mafic and ultramafic bodies in the WGR. This collection shows large variations in petrophysical properties, oxide mineralogy, mineral assemblages, and is discussed in terms of contributions to crustal magnetism. There are four groups of samples, representing different metamorphic conditions and crustal depths: (1) garnet-corona gabbros (CG) considered to have reached 600–750°C and 1–1.5 gigapascal (GPa), equivalent to depths up to 60 km; (2) normal eclogite-facies rocks (HP) that reached 700–750°C and 1.5–2.5 GPa, equivalent to depths of 60–90 km; (3) ultrahigh-pressure eclogite-facies rocks (UHP) that reached 750–850°C and 2.5–4 GPa, equivalent to depths of 90–120 km; (4) mantle peridotites (MP) that may in some places have reached 850–900°C and up to 6.5 GPa, equivalent to depths of 200 km.

2. Lithospheric Magnetic Anomalies From Satellites

The contribution to lithospheric magnetization from deep-crustal rocks remains enigmatic though intermittent studies of this topic span nearly 50 years. The first magnetic anomaly map of the lithosphere was produced in the 1970s based on POGO satellite data (Regan et al., 1975). Later MAGSAT data resulted in global maps of the crustal field (Lowe et al., 2001) followed by the Ørsted, CHAMP, and Ørsted-2/SAC-C satellites with higher resolution data resulting in more advanced models (e.g., Hemant & Maus, 2005; Maus et al., 2006; Olsen et al., 2006; Sabaka et al., 2004). The CHAMP data showed the largest anomalies are over continental crust and magnetic variations of ±30 nT with wavelengths of 400–3,000 km at an altitude of 300 km, the lowest altitude reached by the CHAMP satellite with good global coverage. The new SWARM satellites, with two at low altitude, measuring east-west gradients, and one satellite at higher elevation, are measuring both vector and scalar fields. The coverage and resolution is significantly increased and enables a far more detailed investigation of the deep crust and lithosphere of the Earth.

The most recent model (LCS-1) of the magnetic lithosphere is that of Olsen et al. (2017). This model extends to spherical harmonic degree 185, the highest resolution yet achieved, and is based exclusively

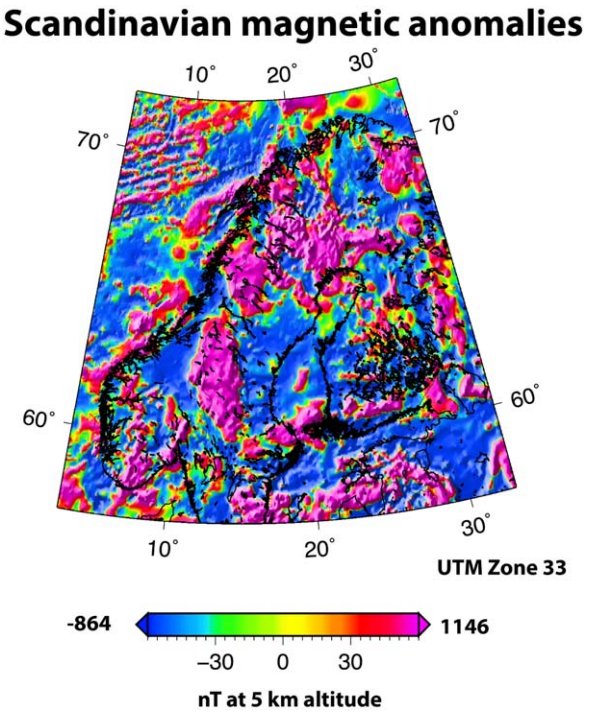

Figure 1. Magnetic anomaly map (total field) of the Scandinavian region at 5 km altitude constructed using the LCS-1 (Olsen et al., 2017) model for the longest wavelengths (in excess of 250 km), and WDMAM-2 (Dyment et al., 2016) for the shorter wavelengths.

on E-W and N-S magnetic gradient data from CHAMP and *Swarm* satellite missions. The high quality of this model is due to the exclusive use of gradient data, data selection, and L1 model regularization of the radial magnetic field at the Earth's surface, modeled as an ellipsoid. Horizontal wavelengths as short as 250 km can be resolved by this model in some locations. For a more complete wavelength rendition of the magnetic field of the lithosphere, we have combined the LCS-1 model with that of the second edition of the World Digital Magnetic Anomaly Map (Dyment et al., 2016) and show the map of Scandinavia (Figure 1). We can place bounds on the minimum value of magnetization required to generate a given set of magnetic field observations using the method detailed in Parker (2003), specifically equation (1). The method assumes a specified magnetic crustal thickness in order to predict the minimum magnetization required to explain the observations, irrespective of the magnetization direction. The method further parameterizes the magnetizations in terms of contributions from elementary dipoles. Parker shows that the integral can be evaluated in elementary terms using a Lagrange multiplier approach, and discovers an analytic expression for the distribution of magnetization that has the smallest possible intensity, without any assumptions about the direction of that magnetization. If we restrict ourselves to the Western Gneiss Region (4.5°E–10°E longitude, 61°N–63.5°N latitude), the absolute maximum value of the lithospheric field is about 363 nT at 5 km altitude.

If we estimate a magnetic crustal thickness of 15 km, the minimum magnetization estimate is about 0.3 A/m (equation (13) of Parker, 2003). Assuming an elongated magnetic source, which may be more in keeping with the strong N-S trending magnetic grain in the eastern part of the WGR, the minimum magnetization estimate is about 0.42 A/m, about 38% greater (equation (14) of Parker, 2003). This is the one-datum problem, and extension to more than a single observation, or eliminating the flat-world approximation, yields only very modest increases in the bounds. Assuming a thicker crust would decrease the magnetization required, and for small changes of thickness the change would scale in a linear sense. If we convert this minimum value to units of susceptibility in the local magnetic field, we find the minimum susceptibility required to create an induced field of this magnitude is approximately 0.01 (SI). In contrast, magnetic susceptibilities of 0.04 (SI) have been used by Thébault et al. (2010) to reproduce the global satellite observations, under an induced magnetization assumption, and using a crustal thickness model (e.g., Mooney, 2007) as a starting point in an iterative approach. This value of magnetic susceptibility, 0.04 SI, is successful in modeling more than 95% of the satellite observations without resort to unphysical (negative) magnetic thickness. In summary, magnetic susceptibilities in the range of 0.01–0.04 SI, and/or magnetizations in the range from 0.4 to 1.6 A/m, given a magnetic crustal thickness of 15 km, can explain the magnetic field observations in the WGR.

Understanding the nature of lithospheric magnetization is challenging, because thermal gradients are a key factor and they are not well known, hence the magnetic crust can vary in thickness from less than 15 to more than 70 km. Over the last three decades there have been limited studies that relate magnetic anomalies to properties of deep-crustal rocks exposed at the surface (Brown et al., 2014; Dunlop et al., 2010; Ferré et al., 2014; Kelso et al., 1993; Liu et al., 2012; McEnroe et al., 1998, 2001a, 2001b, 2002, 2004, 2006, 2007, 2009a, 2009b; Pilkington & Percival, 1999, 2001; Reynolds et al., 1990; Schlinger, 1985; Schmidt et al., 2007; Shive et al., 1992). Many exposures have been subjected to later processes such as retrograde metamorphism (Strada et al., 2006), or serpentinization that can alter the magnetic mineralogy. The new satellites offer increased resolution and sensitivity of the Earth's magnetic field. Clark (1997, 1999) has presented valuable general overviews of magnetic petrology and interpreted this overview in lithospheric studies and models (Purucker & Clark, 2011). Now it is crucial to have detailed studies linking petrology with PT constraints and magnetic mineralogy.

3. Reconstructive Mineral Petrology

There is abundant speculation as to the magnetic behavior of deep-crustal rocks, when they lie at temperatures below Curie or Néel temperatures of their magnetic minerals, after being exhumed from locations of higher-grade metamorphism at greater depth. One approach has been to consider different sets of equilibrium metamorphic minerals that would form under different conditions, assuming that such mineralogy would in fact occur as expected. A second approach is to explore a large area of exposure of rocks, where there is excellent knowledge of the P-T conditions that were reached during peak regional metamorphism, and then to study what has actually happened during this process in terms of magnetic equilibria, mineralogy, and properties. As an example of this second approach, we consider the eclogite-facies terrane of the WGR, Norway, an area of over 28,000 km^2, with outstanding exposures of rocks previously subducted to depths >60 km.

A common approach is to reconstruct mineral assemblages according to a simple understanding of likely mineralogy under different metamorphic-facies conditions, usually backed up by specific natural examples. For example, when an igneous protolith containing abundant magnetite and ilmenite is subject to amphibolite-facies conditions, it is common to find that the magnetic oxides are consumed in the production of new silicates, where Fe^{3+} goes into epidote and hornblende, and Ti^{4+} into hornblende and titanite (Ashwal et al., 1979). In the same or similar rocks, the magnetic oxides may make an important comeback, in the transition from amphibolite facies to the higher-grade pyroxene granulite facies, as in southwest Sweden (McEnroe et al., 2001a).

Similar speculations may involve the transition from high-amphibolite facies or granulite facies to eclogite facies. This transition involves two concurrent processes, production of very abundant garnet from the Fe^{2+}, Mg, Ca, and Al components of other silicates, and breakdown of the sodic component of plagioclase to be incorporated into the jadeite component of the high-pressure pyroxene omphacite. During this the Fe^{3+} of magnetite can be consumed both as an andradite component of garnet, as an acmite component of high-pressure pyroxene, or as a component of epidote or zoisite. In rocks observed in this transition, garnet commonly nucleates earliest on magnetite and ilmenite, which are the minerals richest in FeO (Fe^{2+}) in the rock. Because FeO is transmuted progressively into garnet, remaining TiO_2 eventually becomes rutile. Garnet production in eclogite is the explanation for the abundance of rutile in the Engebøfjell eclogite, now an important ore of rutile (Korneliussen et al., 2000), with metallurgical advantages over rutile sand that tends to have inconsistent geochemistry. A massive deposit of ilmenite in the same region ("ore" samples in HP group), lacking garnet-forming constituents, has remained unchanged through the same eclogite metamorphism. Carried to a logical limit, then, equilibrium eclogite-facies metamorphism of a mafic rock, previously containing magnetic oxides, would contain only Fe-bearing silicates and rutile, and thus be essentially free of magnetic minerals resulting in a dominantly paramagnetic response. In the rocks of the present study this "logical limit" is rarely reached.

3.1. Petrologic Observations in an Eclogite-Facies Terrane

Here we explore the magnetic mineralogy and properties of rocks exposed in one of the world's largest eclogite-facies terranes, the WGR. The extent, pressure-temperature conditions, and timing of metamorphism are summarized below, followed by descriptions of magnetic minerals and magnetic properties of the samples. We show how real metamorphic features differ from theoretical reconstructions. Although these rocks reached depths from 60 up to as much as 200 km and temperatures 750–800°C up to possibly 850–950°C at the very highest pressures, many did not equilibrate to the dominant metamorphic-facies conditions either on the way down to great depth or later on the way back up. Rather, the extent of reequilibration from original gabbro or other mafic mineralogy was dependent on reaction enhancement during local deformation, or during local infiltration of metamorphic fluids. Thus, metastability was rampant, and assemblages purportedly of different metamorphic facies occur within single outcrops, dependent on local deformation features and fluid infiltration along various pathways.

The interiors of many of these bodies show only minor changes of original mineralogy, commonly marked by growth of thin garnet coronas between plagioclase and Fe-Ti oxides or plagioclase and pyroxene or olivine. Two general types of transitions to eclogite-facies assemblages can be observed. Some transitions are produced in eclogite-facies shear zones inside the bodies, or along their margins (Figure 2). In the interiors it is common for the original oxide minerals and plagioclase to be preserved partially, even though garnet growth was proceeding (Figure 3), commonly enhanced by deformation-induced grain-size reduction of reactive minerals, and rutile was being produced from ilmenite. Other types of transitions occurred in a

Figure 2. Fine-grained strongly foliated garnet-rich eclogite in one of three boudins believed to have been torn tectonically from the rim of the Flem Gabbro, Flemsøya. Unfoliated granitic pegmatite showing in the boudin neckline yielded a U-Pb zircon age of 396 Ma (Krogh et al. 2011).

more static environment where fluid-assisted transformation to eclogite has occurred along very sharp diffusion fronts in the gabbro, apparently unrelated to deformation.

Some gabbros, and eclogites derived from them, were overprinted by amphibolite-facies assemblages during exhumation. Local granitic partial melts from surrounding granitoid gneisses invaded extensional openings in eclogites and in gabbros, invariably causing local transitions to amphibolite. Exact sources of the aqueous fluids that accomplished this are still poorly understood. At some localities, it is easy to see amphibolites derived from eclogites, in others, in the same outcrop, it is possible to see amphibolites produced direct from gabbro, with no evidence of the temporally intervening eclogite stage.

4. Importance of P-T Path

Several petrologically inferred or geodynamically modeled P-T paths for domains of UHP metamorphism in the Western Gneiss Region are shown in Figure 4. From the perspective of mineral magnetism, the

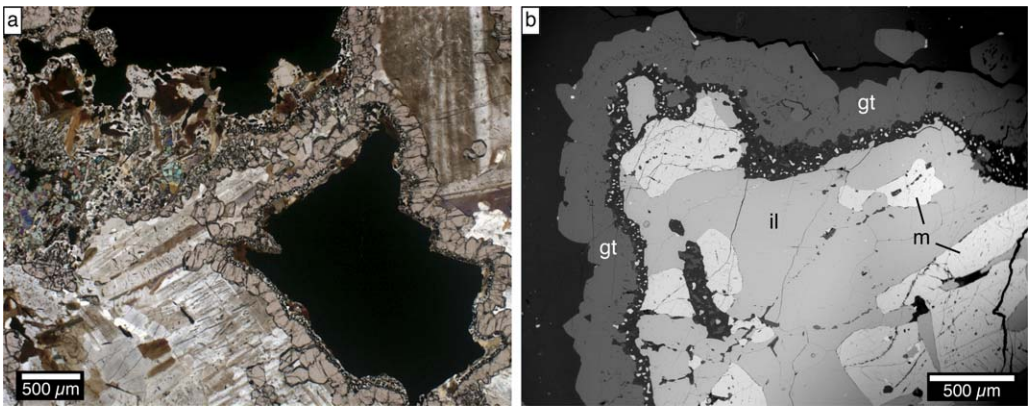

Figure 3. (a) Transmitted light image from HP gabbro. Well-developed garnet rims surrounding oxides are typical. Between garnet and oxides is a very-fine-grained symplectite of plagioclase, pyroxene and magnetite. b) Electron backscatter image of an intergrowth of magnetite (m) and ilmenite (il) surrounded by garnet (gt) and symplectite. Magnetite contains oxy-exsolved lamellae of ilmenite and spinel lamellae.

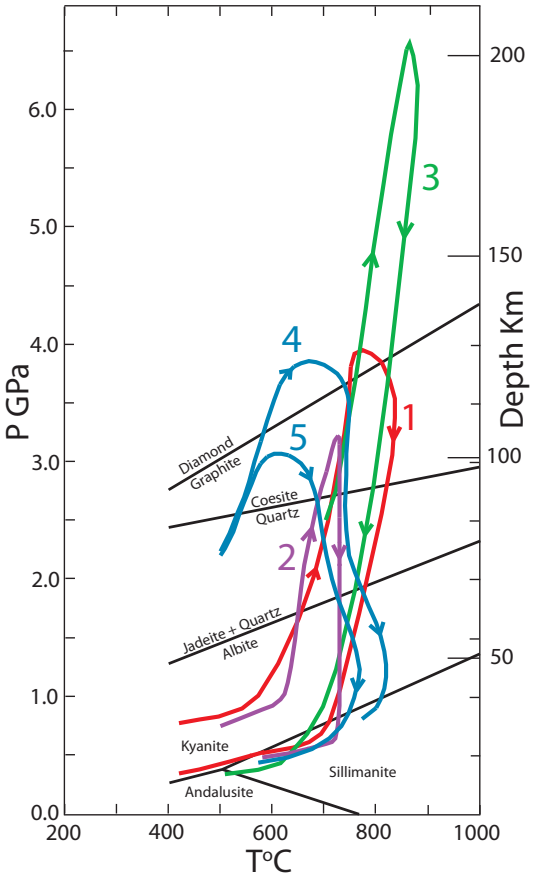

Figure 4. Summary diagram of petrologically inferred and modeled P-T paths for domains of UHP metamorphism in the Western Gneiss Region. Black lines outline important mineral equilibria. From the perspective of mineral magnetism, the concluding parts of all the paths pass through the sillimanite zone at temperatures 800–600°C before cooling through the Curie temperature of magnetite, or exsolution temperatures of rhombohedral oxides. Nevertheless, petrologic phenomena in the earlier parts of the paths could influence the condition of the magnetic oxides upon arrival in the concluding parts. Individual paths are described in the text.

concluding parts of all the paths pass through the sillimanite zone at temperatures 800–600°C before cooling through the Curie *T* of magnetite, or exsolution *T*'s of rhombohedral oxides. Nevertheless, petrologic phenomena in the earlier parts of the paths could influence the condition of the magnetic oxides upon arrival in the concluding parts.

Path 1 constructed by Terry et al. (2008) and Path 2 from Hacker et al. (2010) both show heating to at least 600°C before compression to 3.9 and 3 GPa, respectively, before decompression at high T, over a total interval of 15–20 m.y. Path 3, based on features of peridotites by Spengler et al. (2009), Scambelluri et al. (2008, 2010), and Vrijmoed et al. (2008), go to extreme pressure at high-*T*, but shown here to 850°C, 6.5 GPa, and over a total interval of 35 m.y., before returning to low pressure at ~700°C. Paths 4 and 5 resulted from geodynamic models by Butler et al. (2015) representing conditions of strong (4) and weak (5) lower crust during subduction.

Petrologic paths 1 and 2 begin with initial heating to 600°C, for which there are few petrologic constraints. If this were correct, one could expect high-*T* reactions in the oxides before compression to eclogite facies. By contrast geodynamically modeled paths 4 and 5 stay at lower *T* until at least 2.5 GPa. These may make more sense in terms of what we see in the magnetic oxides. There, many primary igneous features in metamorphosed Proterozoic gabbros are well preserved until garnet-forming eclogite-facies reactions are well advanced at high pressure.

5. Sample Classification Based on Rock Type and Metamorphic Conditions

The collection of mafic and ultramafic rocks from the WGR divides into four groups (Figure 5), not precisely according to rock types, but according to the metamorphic conditions to which the rocks were subjected, based on petrologic studies. This is required because a large volume of rocks, especially massive gabbros, responded only very little toward equilibrium with the applied conditions, and retained many protolith minerals. This metastability was a major lesson learned from the studies of Austreim (1987) and Robinson (1991), applying equally to mineral assemblages and magnetic minerals. Here an important distinction is needed related to grain size of magnetic minerals and their exsolution microstructures. In most occurrences, metamorphic *T*s were high enough to homogenize exsolution microstructures that may have existed in the original igneous or metamorphic protolith minerals. This is shown in an element map of original ilmenite plates from an eclogite-facies mylonitic zone in Haram Gabbro (Terry & Heidelbach, 2004, 2006; Terry & Robinson, 2003). The plates were smeared parallel to the mylonite foliation, so the original ferrilmenites are now in thin streaks crossing nearly the entire thin section. Here there are differently oriented ilmenite subgrains, containing hematite lamellae exsolved at a *T* lower than that of the deformation. Because of the *T*s involved during subduction, primary remanent magnetization was destroyed, and then overprinted during cooling from peak conditions at 415–401 Ma (Krogh et al., 2011). Cooling after the peak *T* occurred at different rates, so magnetic remanence cannot be assumed to be all of the same age. This implies that remanent vectors of mafic bodies in the WGR will vary due to differential cooling rates, different oxide mineralogy and relatively low-*T* deformation of the enclosing rocks (Robinson et al., 2014), resulting in a less-unified vector that lowers the remanent contribution to the magnetic signal.

5.1. Corona Gabbros (CG)

A minority category of 100 samples includes metamorphosed gabbros with garnet coronas implying high-P metamorphism, but lacking evidence for eclogite-facies conditions, 600–700°C and 1–2 GPa. These lie east

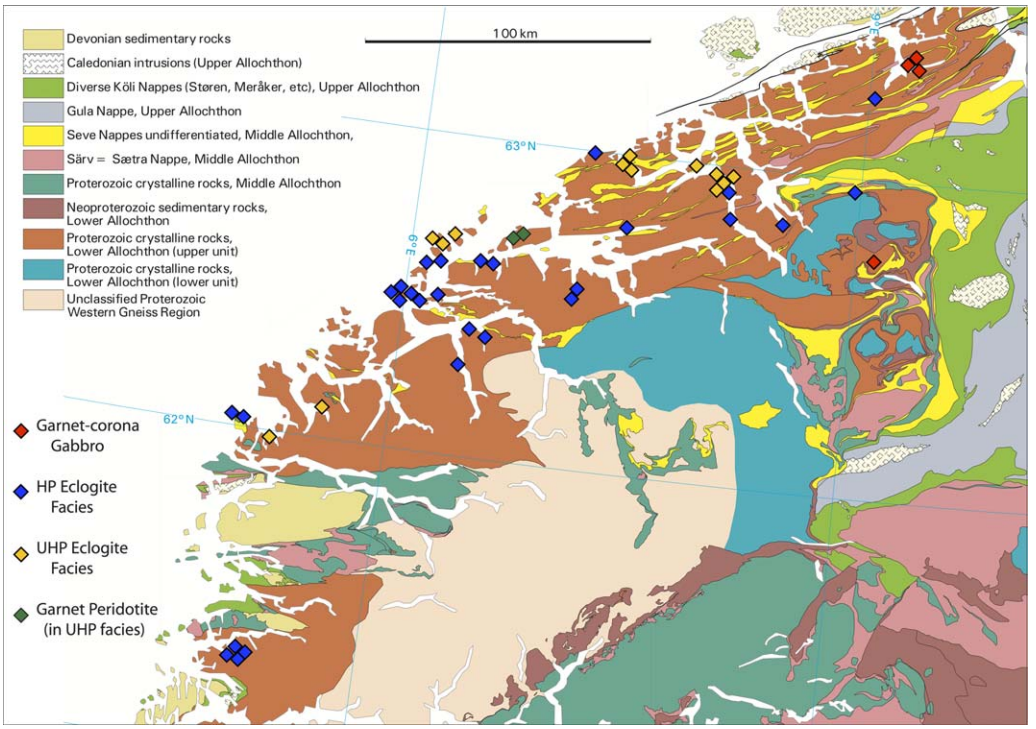

Figure 5. Map of Western Gneiss Region showing general sample locations of corona gabbros (CG, red diamonds), high-pressure (HP, blue diamonds), ultrahigh-pressure (UHP yellow diamonds), and mantle garnet peridotite (MP, green diamonds). Modified from Tucker et al. (2004).

of all known eclogites in Figure 5 (Tucker, 1986) and in one body in deformed basement gneiss in central Trollheimen (red diamonds in Figure 5).

5.2. High Pressure (HP)

A major part of the collection (914 samples) is from areas with evidence of eclogite-facies conditions, implying depths of at least 60 km and temperatures of 750°C, but no evidence of ultrahigh-pressure conditions. Such eclogites may contain primary metamorphic hornblende, which is unstable under UHP conditions (cf. eclogite at Seth, Lepsøya, Terry et al., 2008, dated at 412 Ma, Krogh et al., 2011). Eclogites of the Sunnfjord region (blue diamonds, southern part of Figure 5) are in this group, which is also the only place where pure jadeite was reported (Cuthbert, 1985). The easternmost described eclogites are at Vinddøldalen in northern Trollheimen (Beckman et al., 2014; Tørudbakken, 1982) and SW of Kirksæterøra (Tucker, 1986) (see blue diamonds NE corner, Figure 5). Included in this group is a subset of 20 samples from a hemoilmenite + magnetite ore deposit.

5.3. Ultrahigh Pressure (UHP)

This category consisting of 397 samples is from areas with compelling evidence for ultrahigh-pressure (UHP) conditions, generally >2 GPa and locally reaching 4 GPa. The evidence includes the presence of coesite, or coesite pseudomorphs, reports of microdiamonds, eclogites with low Al orthopyroxene, and phase relations in kyanite and phengite eclogites. Common bimineralic garnet-omphacite eclogites lack sufficient information to give useful *T* and P estimates. Three domains of UHP metamorphism, Nordfjord, Sørøyane, and Nørdøyane (yellow diamonds, Figure 5) have been delineated (Root et al., 2005).

The Nordfjord UHP domain has been most fully studied (Walsh et al., 2007), where coesite was first found (Smith, 1984), and other occurrences were studied (Wain, 1997, Wain et al., 2000), including that at Flatraket. Our collection here is limited to augen gneiss and a metamorphosed mafic dike at Flatraket (Corfu et al., 2014), and metamorphosed anorthosite at Fiskå (Austreim, 2013). Zircon in the Flatraket augen gneiss preserves both igneous protolith ages 1,670–1,640 Ma and a granulite-facies event ~1,100 Ma, and is adjacent to coesite eclogites. The Krakenes Gabbro, W of Flatraket (Corfu et al., 2014), is an olivine corona gabbro

dated at ~1,250 Ma, not firmly characterized as UHP, suggested by estimated conditions $T = \sim$650–700°C, $P = \sim$2 GPa (Lund & Austreim, 2003). Coesite occurs in the Sørøyane UHP domain (Root et al., 2005), where we lack samples, including the Ulsteinvik eclogite (Carswell et al., 2003; Tucker et al., 2004).

The Nordøyane UHP domain was first indicated by reports of metamorphic microdiamonds in kyanite-garnet gneiss at Fjørtoft (Dobrzhinetskaya et al., 1995), then in garnet peridotite at Fjørtoft (van Roermund et al., 2002) and finally in metasomatized spinel peridotite at Svartberget (Vrijmoed et al., 2006, 2008). The Fjørtoft garnet peridotite also gave evidence for a former majorite component in Scandian garnet (Scambelluri et al., 2008). Coesite pseudomorphs occur in eclogite on Fjørtoft and Flemsøya, also with phase relations consistent with UHP conditions (Terry et al., 2000). Actual coesite inclusions in eclogite garnet occur on Harøya (Butler et al., 2012).

Nearly all the UHP mafic samples are from the Nordøyane domain. The southern domain boundary is sharply defined for 60 km E-W on islands by the amphibolite-facies Åkre and Midsund mylonite zones (Krogh et al., 2011; Terry & Robinson, 2003), presumed to extend E ~70 km into the mainland. The northern boundary is crudely located N of Nordøyane and presumably extends east toward Kristiansund. The eastern limit is unknown, perhaps due to the high *T*s that destroyed scarce indicators of UHP metamorphism. The Averøya eclogites (63°N in Figure 5) suggest likely UHP conditions (Auglænd, 2017; Auglænd et al., 2017). We think that rocks metamorphosed to UHP may extend E at least to Kristiansund, thus including much of our collection.

5.4. Mantle Peridotite (MP)

This category includes ultramafic rocks with a complex and uncertain history. All 90 of our samples come from three mantle bodies, at Ugelvik and Raudhaugene on Otrøy (Brueckner et al., 2010; Carswell, 1973; van Roermund, 2009; van Roermund & Drury, 1998; Spengler et al., 2009), and Kvalvika on Flemsøy (Terry, 2010; Terry et al., 2005). Their history involves Archean and Proterozoic processes in the deep mantle before Scandian metamorphism, including production and later breakdown of a supersilicic majorite component in garnet, shown by pyroxene exsolution lamellae. These, and a small body on Fjørtoft contain occurrences of giant Al-rich orthopyroxene (Carswell, 1973; Terry et al., 1999), thought to have formed during upward flow in a Proterozoic mantle plume, later exsolved to a mixture of lower Al orthopyroxene, Cr diopside, and garnet. Spengler (2009) reported extremely low Al orthopyroxene in Scandian shear zones in the peridotites, indicating metamorphic conditions to 6.5 GPa suggesting depths to 200 km, constrained by Sm-Nd mineral isochrons at ~430 Ma, older than the 415–401 metamorphic ages of eclogites (Krogh et al., 2011).

The small Kvalvika body (Terry, 2010; Terry et al., 2005) contains a "low-*T*" olivine fabric consistent with deformation at ~800°C, parallel to a steep Scandian eclogite-facies fabric in surrounding gneisses. That fabric is dated at ~410 Ma by the eclogite-facies margin of the nearby Flem Gabbro included in our UHP collection. Terry gives petrologic evidence for a P-T path passing through ~4 GPa appropriate for microdiamond stability. The garnet peridotites were serpentinized under low-*T* conditions long after any ductile deformation. These reactions produced little magnetite, possibly due to the high Mg content of the olivine.

6. Transmitted and Reflected-Light Microscopy and Electron Backscatter Images

Sample locations were picked based on previous petrographic and petrologic studies cited above. Thin sections were observed to check the earlier descriptions and to describe the oxides. If samples were altered, this was noted. Most samples have only minor alteration, except for the mantle peridotite samples, which commonly show effects of low-T serpentinization.

The variety of oxides and microstructures found in the WGR is striking especially in the HP and UHP rocks. The oxides and their microtextures, are divided into three groups: (1) magnetite, and magnetite with oxidation exsolution of ilmenite (Figure 6); (2) exsolved rhombohedral oxides; ilmenohematite and hemoilmenite (Figure 7), and (3) oxides formed in symplectite reactions and in mylonites (Figure 8).

6.1. Magnetite, and Magnetite With Oxidation Lamellae of Ilmenite

Magnetite is present in some samples from all four groups (CG, HP, UHP, and MP) though not in all. It is very rare in samples that have converted completely to eclogite. Figure 6a is an electron backscatter image showing rare magnetite and ilmenite in a coarse orthopyroxene eclogite from the UHP region on Øtrøya.

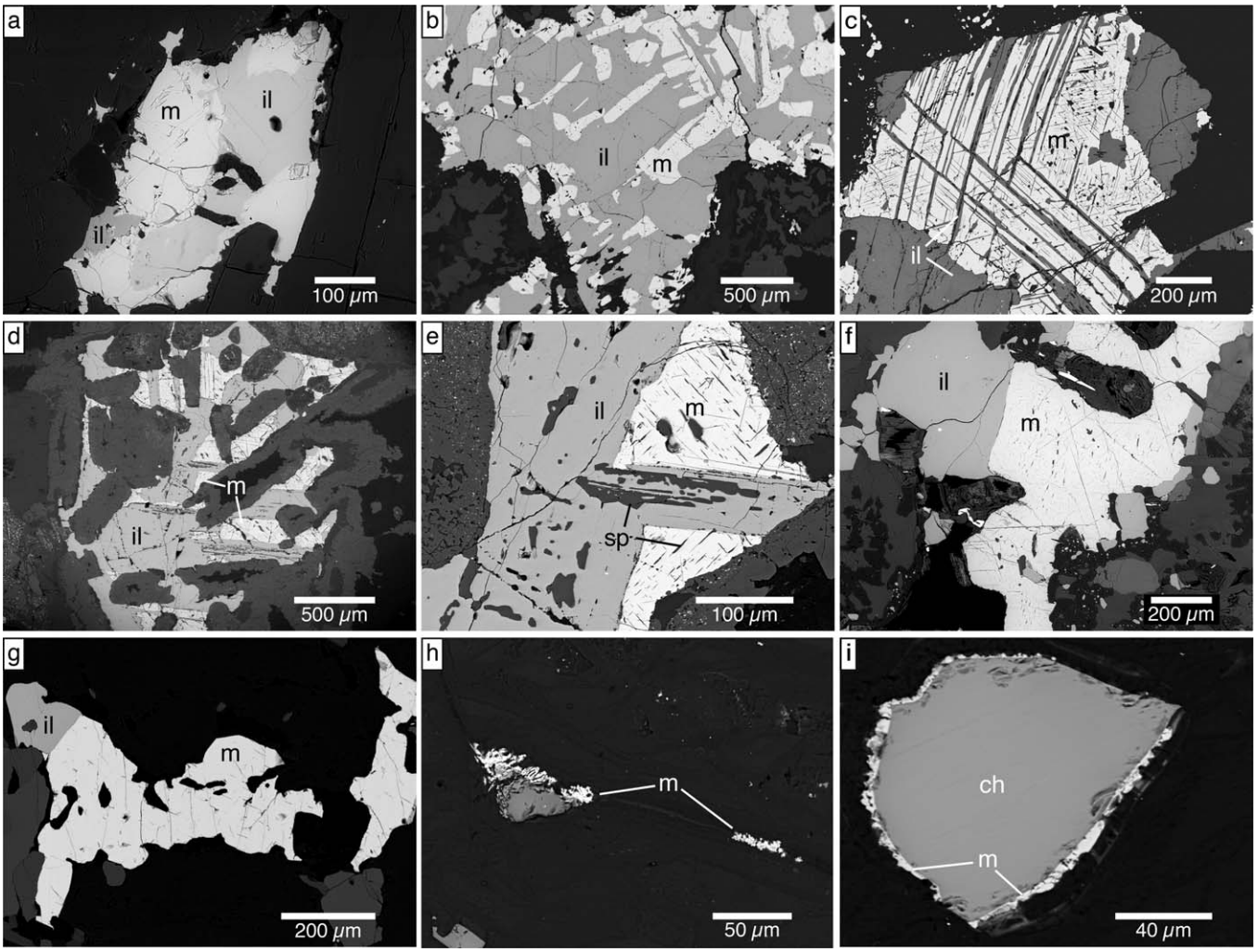

Figure 6. (a–i) Electron backscatter images of magnetite, (b–f) magnetite with oxidation-exsolution lamellae of ilmenite from CG, HP, UHP rocks. Spinel in ilmenite and magnetite in Figure 6e is an enlarged image of Figure 6d to show exsolution features. Fine secondary magnetite in MP shown in Figures 6h and 6i. m: magnetite, sp: spinel, il: ilmenite, ch: chromite.

The magnetite contains {111} oxidation-exsolution lamellae of ilmenite but the ilmenite grains lack exsolution.

Magnetite is most common, in fact ubiquitous in the corona gabbro samples. The magnetite grains are large, in the multidomain (MD) region of magnetite (>20 μm). Figures 6b and 6c are from the Botnvatnet corona gabbro in Trollheim. The magnetite-ilmenite intergrowth in Figure 6b has an unusual morphology of isolated magnetite grains within a large ilmenite (>500 μm) and some magnetite contains minor oxidation exsolution of ilmenite, and spinel needles or blades. In Figure 6c, the magnetite is in direct contact with garnet, and it appears garnet is replacing ilmenite lamellae. Within the magnetite there are abundant small exsolved {100} spinel needles.

In HP and UHP gabbro samples magnetite is less abundant. The discrete magnetite grains typically are very large multidomain-size grains, and contain oxidation-exsolution lamellae of ilmenite, and spinel lamellae shown in Figures 6d, 6e, and 6f. The ilmenite lamellae commonly contain blebs of spinel (Figure 6e) that may, or may not be topotactic. In some samples magnetite may only contain spinel lamellae, and have coexisting discrete ilmenite grains (6f). Figure 6g shows an unusual garnet magnetite rock in HP region from Godøya. The magnetite grains are large with few exsolution features except minor spinel lamellae.

In the mantle peridotite samples, magnetite is rare except where formed in retrograde serpentinization. Commonly magnetite occurs along cracks and grain boundaries (Figure 6h), contains no oxidation-

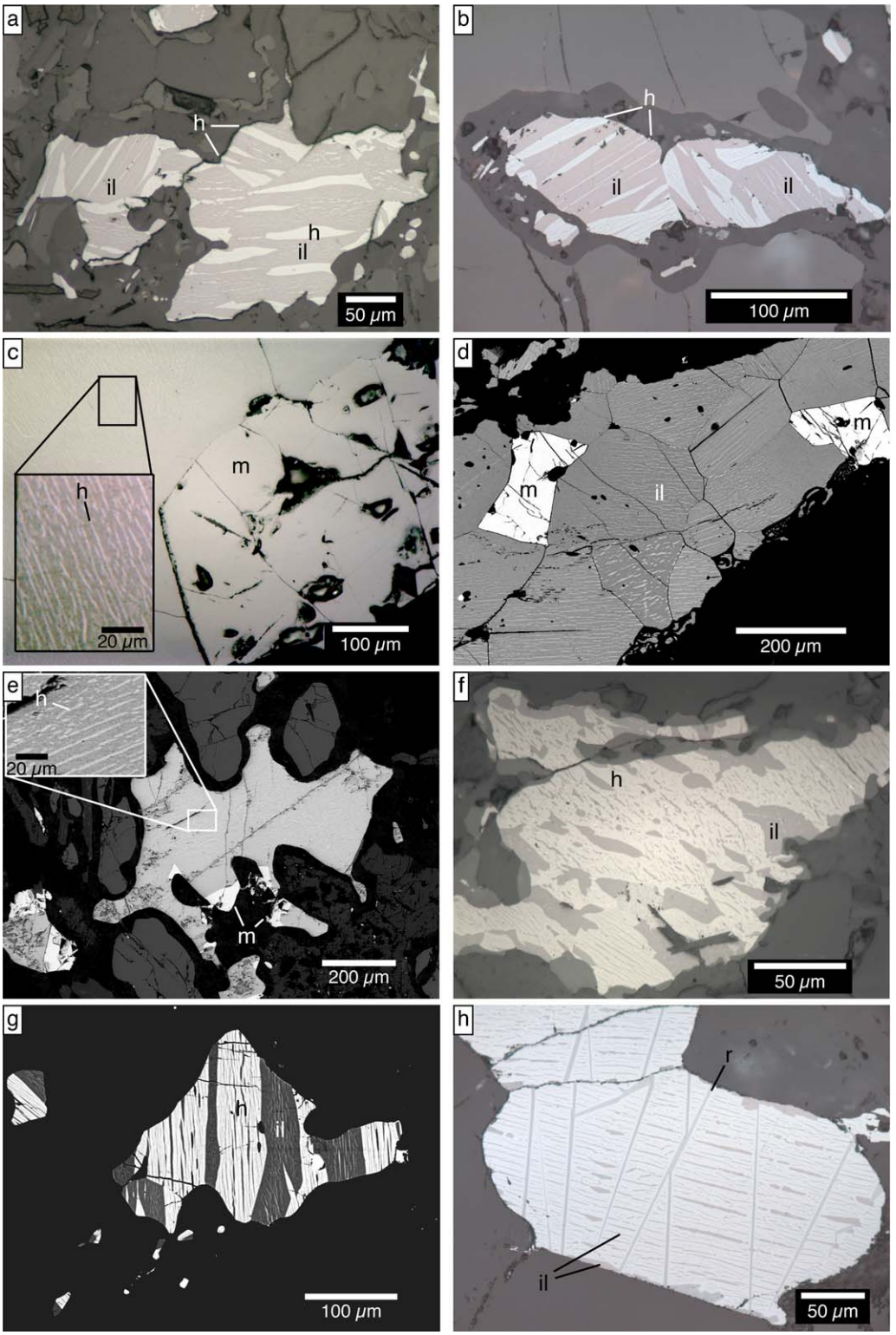

Figure 7. (a, b, f, and h) Reflected-light and (c, d, e, and g) electron backscatter images of rhombohedral oxides in HP and UHP samples, including some samples with coexisting magnetite. Ilmenite with hematite exsolution lamellae (hemoilmenite) shown in images (a–d), and hematite with ilmenite exsolution lamella (ilmenohematite) in images (f–h). In Figure 7h, the ilmenohematite also contains exsolution blades of rutile (r). m: magnetite, sp: spinel, h: hematite, il: ilmenite samples described in text.

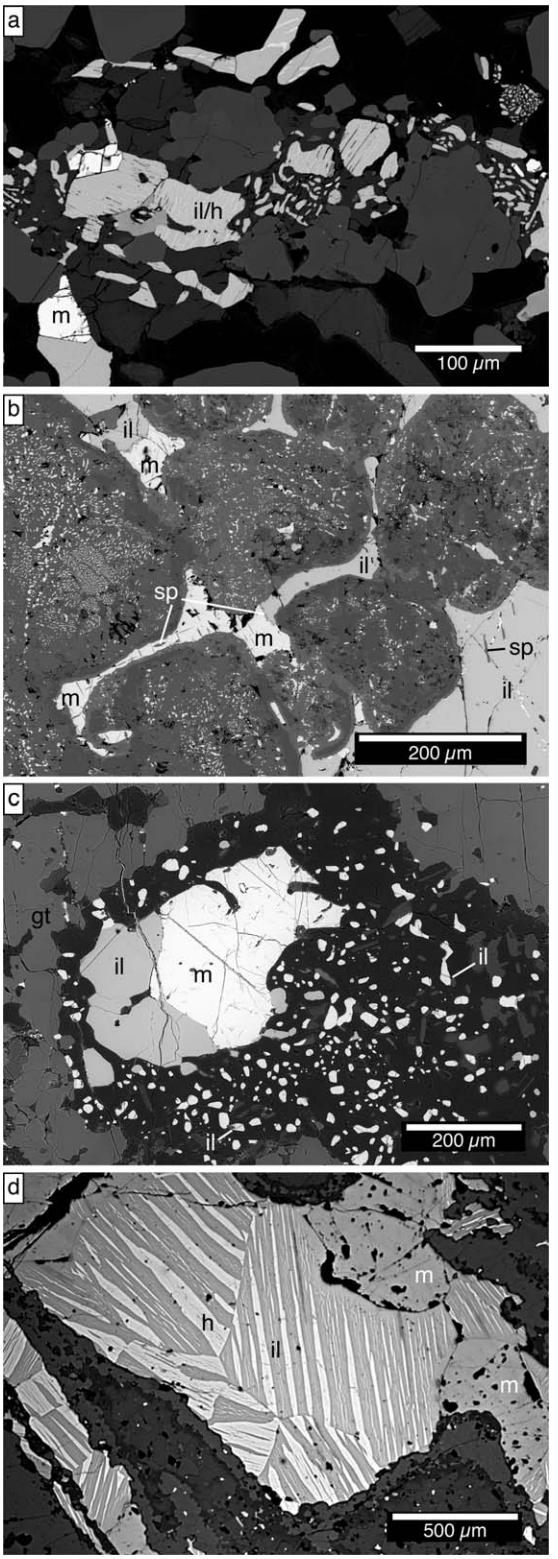

Figure 8. Electron backscatter images showing symplectite textures in (a) HP, (b and c) UHP samples and (d) reflected-light image of ilmenite and magnetite in mylonite from Flem Gabbro (HP). m: magnetite, sp: spinel, h: hematite, il: ilmenite.

exsolution lamellae, or microstructures and ranges in size from a few microns to >20 μm. Figure 6i shows a magnetite rim on chromite, or Cr-spinel with Al, Mg substitution (Strømøy, 2014). Though it is ubiquitous in many samples, the amount of magnetite associated with chromite, is very small. Most of the magnetite observed in peridotite thin sections was formed by late low-*T* serpentinization. The magnetite rims on chrome spinel, formed at an unknown stage.

6.2. Rhombohedral Oxides

The rhombohedral oxides in the hematite-ilmenite solid solution ($FeTi0_3$-Fe_20_3) series (Figure 7) show exsolution lamellae that would have formed at *Ts* below that of the peak metamorphism (800–850°C). These occur in numerous HP and UHP rocks, though not in the mantle peridotites, nor should we expect such oxidized assemblages there. The absence of the exsolved rhombohedral oxides in the collection of garnet-corona gabbros is likely due to the small 100 sample collection compared with the large 914 sample HP and large 397 sample UHP collections. There is no obvious petrological reason for their absence in the CG samples. The presence of rutile in the Botnvatnet corona gabbro indicates that hemoilmenite may have been present at an early metamorphic stage, and was reacted out during higher *T* metamorphism.

Exsolved rhombohedral oxides are common in many intermediate to mafic igneous intrusions and in granulite-grade rocks studied elsewhere (Brown & McEnroe, 2008; Dyar et al., 2004, McEnroe & Brown, 2000; McEnroe et al., 1996, 2001a, 2001b, 2002, 2007, 2009a, 2001b; Robinson et al., 2002). They can be strongly magnetic, due to uncompensated moments at the interfaces of the two phases (McCammon et al., 2009; Robinson et al., 2002, 2004, 2016).

Both hemoilmenite and ilmenohematite grains vary in size from a few microns to >100 μm. The exsolution lamellae (ilmenite in hematite (ilmenohematite), or hematite in ilmenite; hemoilmenite) are generally SD size (<10 μm). Small grains <5 μm with exsolution lamellae are can be present as inclusions in silicates. In the CG samples, magnetite and ilmenite are typically rimmed by garnet, in contrast to rhombohedral oxides at HP and UHP conditions where this relationship is not so common.

Figure 7 shows HP and UHP samples containing hemoilmenite (Figures 7a–7e) and ilmenohematite (Figures 7f–7h). Hemoilmenite with an initial bulk composition relatively rich in a hematite component prior to exsolution is shown in Figure 7 from the HP Vinddøldalen gabbro that also contains magnetite (Figure 7a) and from a UHP gneissic rock (Figure 7b) from Averøya. These samples typically have abundant coarse exsolution lamellae. The ilmenite host grains (darker) with hematite exsolution lamellae (lighter) parallel to (0001), and with second and subsequent generations of hematite lamellae also parallel to (0001) shown in Figures 7a and 7b is a feature that will enhance the remanent magnetization. These exsolution features are very similar to those found in high-grade metamorphosed gabbros in the SW Sweden granulite region (McEnroe et al., 2001a) in a region where eclogites have been discovered (Möller, 1998). Finely exsolved hemoilmenite was found in numerous localities in the HP group (Figures 7c and 7d) and commonly occurs with minor magnetite. The UHP

country rock gneiss adjacent to the Ørtøya garnet peridotite contains hemoilmenite (Figure 7e) with fine-scale hematite exsolution lamellae that appear to be only one generation, however hematite lamellae may be below the optical limit of the microscope, and in the superparamagnetic grain-size range. Adjacent to the hemoilmenite is a large magnetite grain, with minor spinel exsolution and spinel symplectite at the border of the two grains. The morphology of the hemoilmenite suggests disequilibrium with distinct embayment features.

Other HP gabbros contain titanohematite with ilmenite exsolution, which also contains later hematite exsolution (Figures 7f and 7g). These assemblages are more hematite-rich than those in Figures 7a and 7b. A gneissic rock adjacent to the UHP Averøya eclogite contains titanohematite, which is rimmed by garnet. The titanohematite host contains exsolved rutile blades and ilmenite lamella (Figure 7h). The original bulk composition would have been very rich in Fe^{3+}, which likely had a sedimentary protolith. In the titanohematite are fine ilmenite exsolution lamellae parallel to (0001) and some contain very-fine rutile lamellae. Second-generation hematite lamellae exsolved from the larger ilmenite lamellae are also parallel to (0001). Subsequent generations of lamellae are below the limits of optical resolution. This assemblage is very similar to that found in a granulite-facies sillimanite gneiss in the NW Adirondacks, USA (McEnroe & Brown, 2000) and in the upper-amphibolite facies in Modum Norway (McEnroe et al., 2007, 2016).

6.3. Symplectite Reactions

Numerous CG, HP, and UHP samples show evidence of oxide-silicate symplectite reactions, which produced oxides upon cooling or decompression. Both magnetite and hemoilmenite are common products in these reactions (Figures 8a–8c). Magnetite commonly has minor {111} oxidation-exsolution lamellae of ilmenite, and exsolution of spinel as blades, or needle-shaped lamellae. The oxides are small, usually only a few microns (Figures 8b and 8c) and, with the grains subdivided by lamellae, the magnetite grains are in the pseudosingle-domain-size to single-domain-size range.

The symplectites in Figures 8a–8c, from HP and UHP samples, represent reactions that took place during late-stage decompression. The oxidation exsolution of ilmenite from magnetite, and the exsolution of the hematite from the ilmenite, or ilmenite from hematite would have taken place at lower temperatures than the peak metamorphism. Based on a calculated room-pressure Fe_2O_3-$FeTiO_3$ phase diagram (Harrison et al., 2006), ilmenite-rich compositions close to Ilm 60 could separate into hematite-richer and ilmenite-richer compositions at as high temperatures as 800–700°C. However, the hematite-richer phases would remain paramagnetic until progressive exsolution brought them to the 520°C eutectoid composition at about Ilm 20 where CAF (canted-AF) hematite could exsolve. For compositions more hematite-rich than $ilmenite_{20}$, Ti-rich ilmenite could only exsolve at the 520°C eutectoid, or below. Various experimental and theoretical considerations (McEnroe et al., 2004, 2007, 2008) suggest that all these temperatures could be higher at a pressure of 1 GPa. Thermal demagnetization experiments on hemoilmenite, with hematite lamellae of composition Ilm 14, yielded a hematite Néel T of 600–610°C (McEnroe et al., 2007), which is about 25°C higher than predicted for a single-phase hematite of the same composition. The temperature constraints on the ilmenite oxidation-exsolution lamellae in magnetite are less well known, but it is clear that the magnetite in the symplectite formed in a decompression reaction upon cooling.

6.4. Mylonite Samples

Hemoilmenite and magnetite are found in numerous mylonite samples in the region. Figure 8d shows hemoilmenite and magnetite from oxide grains drawn out along the foliation in a mylonite derived from the Haram Gabbro, originally studied by Terry and Robinson (2003). The oxides acquired a nearly continuous rim of fine-grained garnet during deformation and UHP metamorphism. This process likely extracted FeO from the oxide, yielding a magnetite with lower Ti content, an ilmenite with higher hematite content, and locally very small patches of rutile. During cooling from the peak metamorphic conditions of shearing, hematite lamellae exsolved from ilmenite, where the lamellae themselves show no evidence for the earlier intense shearing (Figure 8d).

7. Rock-Property Measurements

A combination of measurements was used to investigate petrophysical properties of the sample collection throughout the WGR, and to understand better the nature of the magnetic oxides residing at depths in the

crust at these metamorphic conditions. We also attempt to describe the heterogeneity that likely exists at depth, and how these results may be applied to crustal-scale geophysical interpretations.

7.1. Methods

Samples were collected as oriented blocks and later drilled in the laboratory, or drilled and oriented in the field. Specimens were then cut to approximately 2.5 cm long cores with a 2.54 cm diameter. Oriented specimens (1,501) were measured for natural remanent magnetization (NRM), susceptibility (*k*), and density. NRM was measured using a JR-5 magnetometer, or a 2G 3-axis cryogenic magnetometer.

For susceptibility, an SI2B Susceptibility Bridge with an operating field of 80 A/m, or an AGICO Kappabridge, with a field of 200 A/m was used and both data sets were normalized to operating field. Susceptibility values are reported in SI units (k) and are dimensionless. For density measurements, samples were soaked for a minimum of 24 h in water, towel dried, and their dry and wet mass measured. Densities were calculated using a Mettler Toledo ML104 scale with a density kit, or at the petrophysical lab at Geological Survey of Norway. For comparing the susceptibility, induced magnetization and NRM values samples must be either weight, or volume normalized. All data presented here are volume normalized.

To characterize the magnetic oxides further, measurements were made on a Princeton Applied Research vibrating sample magnetometer (VSM) in a maximum field 1 T. Hysteresis loops and backfield remanence curves provide data on saturation magnetization (Ms), remanent saturation magnetization (Mr), coercivity (Hc), and coercivity of remanence (Hcr) properties. Electron microprobe data and SEM images were collected on the silicates and oxides from selected samples to gain further insights into metamorphic reactions and resulting magnetic properties.

7.2. Summary of NRM, Susceptibility, Density

The magnetic properties of the samples vary significantly by rock type (GC, HP, UHP, and MP). Within-rock-type and summary data are given in Table 1. The important quantities from the perspective of magnetic anomalies are NRM and susceptibility. Figure 9 is a box plot with data sorted according to the four rock types. The bounds of each box show the 25th and 75th percentiles. Within each box a black line shows the median while a red line shows the arithmetic mean of each group. Outliers are plotted as circles. The data set has a range in NRM values of 0.1 mA/m to 60 A/m, but excluding the ore samples, only values up to 20.4 A/m. Susceptibility ranges from 0.0001 to 1.02 SI (to 0.323 excluding ores). Densities range from 2,385 to 4,736 kg/m^3 (to 3,836 kg/m^3 excluding ores).

Table 1
NRM (A/m, Susceptibility (SI) and Density of Corona Gabbros, High Pressure, Ultrahigh-Pressure, and Mantle peridotite Samples

	Mean	Min	3%	25%	Median	75%	97%	Max
NRM (A/m)								
CG	0.6866	0.0220	0.0373	0.1750	0.5291	0.9352	2.4316	5.5230
HP	1.0756	0.0001	0.0010	0.0260	0.1473	0.6046	5.7611	60.5030
HP*	0.5708	0.0001	0.0010	0.0253	0.1408	0.5699	3.0882	20.3850
UHP	0.9142	0.0008	0.0050	0.0425	0.1720	0.5031	8.0948	18.9000
MP	0.1867	0.0020	0.0033	0.0311	0.0520	0.1935	1.6081	3.3331
Magnetic Susceptibility (SI)								
CG	0.03998	0.00222	0.00307	0.02644	0.03737	0.05032	0.10590	0.11000
HP	0.03625	0.00011	0.00048	0.00123	0.01019	0.04050	0.15302	1.02060
HP*	0.02546	0.00011	0.00047	0.00121	0.00921	0.03845	0.11291	0.32315
UHP	0.01629	0.00006	0.00073	0.00234	0.00878	0.02014	0.07608	0.12081
MP	0.00123	0.00038	0.00054	0.00063	0.00093	0.00140	0.00399	0.00600
Density (kg/m^3)								
CG	3057	2909	2947	3017	3057	3100	3156	3180
HP	3156	2674	2806	3063	3144	3240	3450	4736
HP*	3142	2674	2805	3065	3144	3239	3403	3836
UHP	3156	2654	2775	3066	3159	3236	3490	3525
MP	2789	2385	2529	2656	2700	2932	3190	3460

Note. Statistics of HP rock type calculated including and excluding ore samples, indicated HP and HP*, respectively.

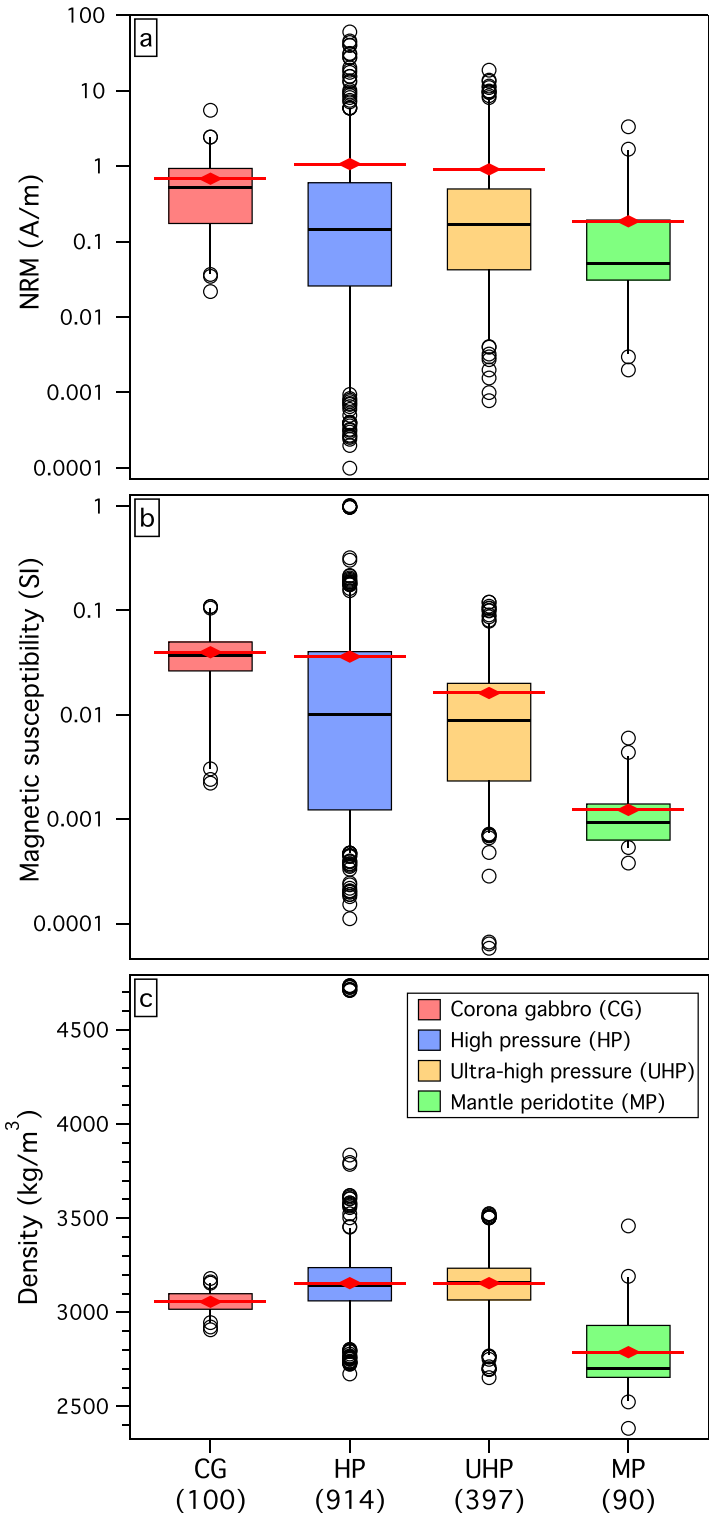

Figure 9. Box and whisker plots of NRM, susceptibility, and density, divided by rock type. Plots show 3, 25, 50 (median, heavy black line), 75, and 97 percentiles, as well as outlying specimens. Also shown are arithmetic mean (red diamond). Complete data set for HP samples shown; distributions excluding commonly outlying ore specimens found in Table 1 and discussed in text.

The garnet-corona gabbros (CG) show a range in NRM values from 22 mA/m to 5.52 A/m). The mean and median values are similar at 0.69 A/m and 0.53 A/m, respectively. The HP samples (excluding ores, here and below) have a similar mean NRM of 0.57 A/m though a significantly lower median of 0.14 A/m. UHP samples have a significantly higher mean of 0.91 A/m with a median of 0.172 A/m. Both HP and UHP samples have non-Gaussian highly skewed distributions with a subsidiary group of highly magnetic samples raising the mean value. The MP samples have the lowest NRM values, with a mean at 0.187 A/m and a median at 0.052 A/m.

The susceptibility values of the garnet-corona gabbros (CG) also show the highest median at 0.0374 SI and mean at 0.040 SI). The HP and UHP groups show similar median susceptibilities at 0.0092 SI and 0.0088 SI, respectively), but the HP group shows a higher mean susceptibility at 0.026 SI compared to UHP at 0.017 SI. The MP samples have the lowest mean and median susceptibilities at 0.001 SI.

The garnet-corona gabbros (CG) show a tight cluster in density values with a similar mean and median of 3,057 kg/m^3. This mean is lower than the HP group at 3,142 kg/m^3 and the UHP group at 3,156 kg/m^3, consistent with the fact that a smaller proportion of their plagioclase has been converted to garnet and omphacite during high-pressure metamorphism, and the larger variation in bulk compositions in the HP and UHP samples. The dominant low densities of the MP samples with mean at 2,789 kg/m^3 and median at 2,700 kg/m^3, respectively, show the effect of significant serpentinization.

However, unlike other strongly serpentinized ultramafic bodies, such as the Leka Ophiolite (Michels et al., 2015), this process has not led to major production of magnetite. These samples have low NRM and susceptibility values, likely due to the Mg-rich initial bulk compositions of the olivine, with less Fe available to react to produce magnetite during serpentinization. However, the large density ranges in the data set with mean values of 2,385–3,836 kg/m^3, excluding the HP ores at over 4,500 kg/m^3, demonstrates that a variety of rock types, as well as prograde and retrograde effects were involved.

Figure 10 shows kernel density estimations that give a more complete picture of the underlying distributions and shows the bimodal nature of some of these data sets more clearly than the box plots. The probability density plot of NRM shows limited, albeit skewed, deviation from log-normal distributions. The MP and UHP sample sets have secondary components that form shoulders in the curves approximately one decade below and above the main peak, respectively. The UHP samples have the most distinct grouping at 0.23 and 3.85 A/m, where many with higher NRMs have mixed oxide assembles, or symplectite reactions producing oxides. Most rock types are clearly bimodal in susceptibility. The CG samples have a higher population at 0.04 SI, and a subsidiary group at 0.0035 SI. The HP group is divided into a very low population at 0.0012 SI, and a higher one at 0.032 SI. The UHP group also shows a magnitude of order difference at 0.0014 and 0.014 SI. These differences reflect initial bulk compositions, and more directly magnetite content. In density, the MP clearly shows two populations reflecting the amount of serpentinization, whereas the CG is distinct with a unimodal density peak at 3,060 kg/m^3. The UHP rocks show two peaks at 3,150 and 3,395 kg/m^3.

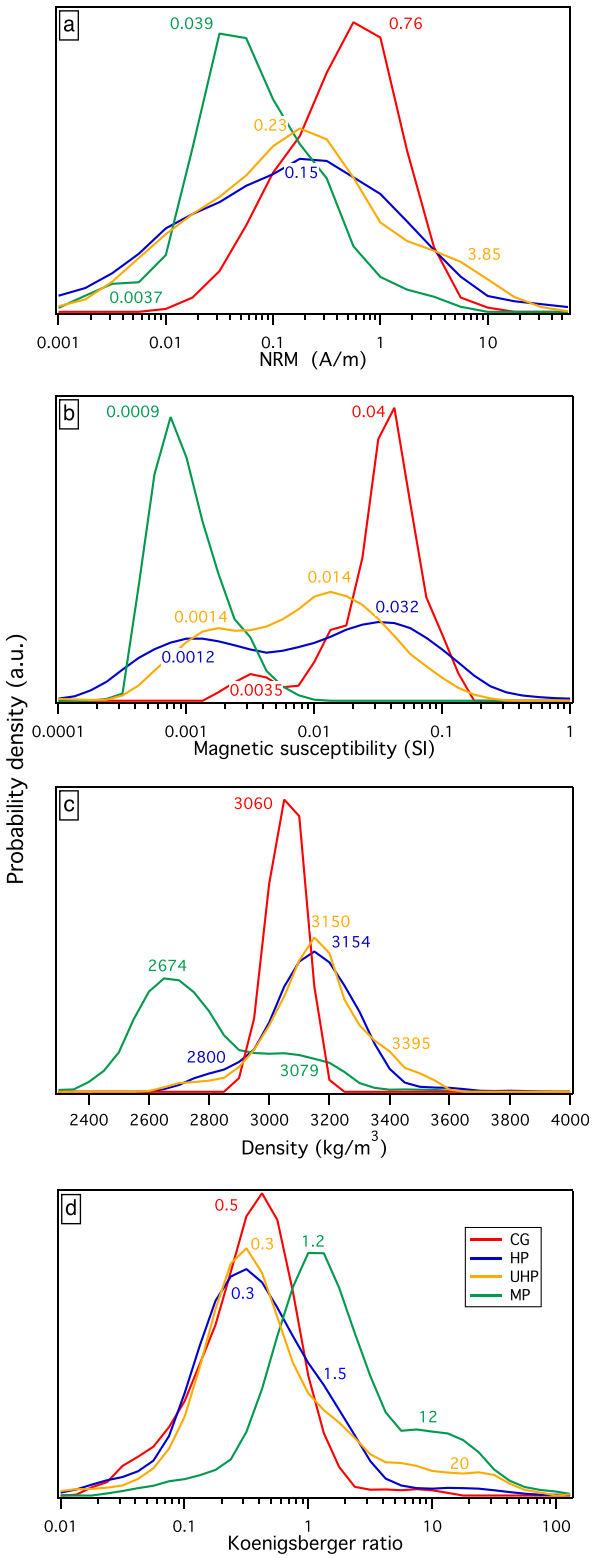

Figure 10. Kernel density estimation (KDE) of NRM, susceptibility, density, and Koenigsberger ratio by rock type. Colored values are centers of primary and secondary peaks, calculated as sums of 2–3 overlapping log-normal (Gaussian in Figure 10c) distributions fit to KDE data. Vertical axes are arbitrary units, with the same scale used within each subfigure.

7.3. NRM Versus Susceptibility

Figure 11 is a plot of NRM in A/m versus magnetic susceptibility (SI) on the top axis. The HP and UHP sample sets show a wide range of NRM and susceptibility values, while CG samples are more strongly clustered. The MP samples plot in a high concentration at low susceptibilities ~0.001 SI and primarily have NRM values between 0.001 and 0.1 A/m, with three outliers above 1 A/m. The CG samples, by contrast, are most densely clustered in a region with higher susceptibilities >0.04 and NRM values between 0.1 and 1 A/m. There is some scatter in both data sets, notably in susceptibility values of the CG samples.

In general, the overall trend of the compiled four data sets is a linear increase in NRM with increasing susceptibility. Due to magnetite's high intrinsic susceptibility and role as an NRM carrier in many samples, this trend largely reflects the concentration of magnetite. On this log-log plot the linear correlation coefficient is 0.747, and r^2 of 0.56, showing that just over half of the NRM variance is controlled by susceptibility. Samples lying outside the densely clustered area are likely to have magnetic mineral properties not characteristic for the data set as whole, such as exceptionally small or large magnetite particles, or nonmagnetite remanence carriers. Deviation from the linear magnetite concentration trend largely reflects either the presence of exsolved members of ilmenite-hematite solid solution, and/or very-fine magnetite grains usually resulting from symplectite reactions. Exsolved rhombohedral oxides have significantly lower susceptibility than magnetite, and can have a strong remanence. Their presence in some HP and UHP samples may explain the greater deviance of those data sets, from the magnetite trend, than that of the CG samples, which contain only magnetite. For example, the reduced chi-square of HP and UHP sets is 2 and 3 times, respectively, that of CG data set. The spread in NRM values in MP samples with similar susceptibilities likely results from varying amounts of fine-grained magnetite, which is a more efficient remanence carrier than coarse-grained magnetite.

The bottom axis of Figure 11 is the derived quantity, induced magnetization (Mi), which approximates the magnetization of samples in situ in the crust, in response to the Earth's local geomagnetic field. It is calculated as the product of the measured low-field susceptibility and the local field by

$$\mathrm{Mi} = k * \mathrm{H},$$

with induced magnetization (Mi) in A/m, and where k is volume-normalized susceptibility and H is the local field in A/m. The geomagnetic field for the WGR is 51,256 nT (IGRF-2012, equivalent to 41 A/m), and varies by <2% in the region discussed here.

Because induced magnetization can have a significant, but sample-dependent, contribution to the total magnetization, the Koenigsberger ratio (NRM/Mi, also called Q value) is used to estimate the relative contribution of these two components and inform on the dominant response of the rocks, i.e., remanent versus induced. The sum of the *Mi* and NRM vectors is the total magnetization (direction and intensity) and results in magnetic field anomalies, which can be positive or negative, i.e., above, or below background, respectively. Plotted on the graph in Figure 11 are lines of constant Q value. Generally, for Q < 0.5, induced magnetism will be dominant, whereas when

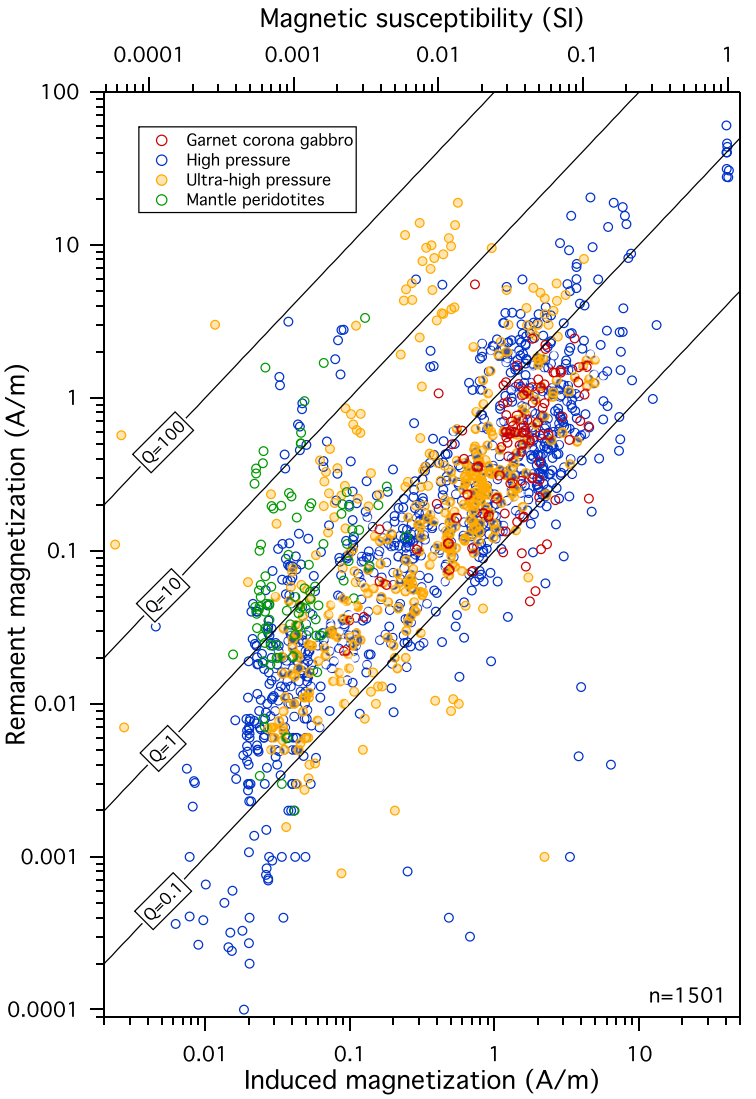

Figure 11. (top axis) Plot of NRM as function of susceptibility and (M_i, bottom axis) induced magnetization calculated for WGR. Lines of equal Koenigsberger ratio (NRM/M_i, or Q value) indicated for decadal ranges from 0.1 to 100.

$Q \geq 0.5$, NRM direction increases in importance, and for $Q > 2$, NRM will dominate at the sample level. However, in a rock body, the bulk NRM is a vector summation, and the amount of scatter or alignment of the NRM directions is important. For each body, a vector Q_v can be calculated by vectorially averaging all the NRM data, and Q_v will always be lower than the scalar Q, because this calculation takes into account both the direction and intensity of the NRM in the vector summation. Here we are examining an area of 28,000 km^2, with differential cooling histories resulting in long acquisition times for the NRM, and variations in oxides and microstructures that will affect domain states. For this reason, there is more scatter in NRM directions than if we were examining only one of the studied localities. Though the vector Q is not used here, this data is still of use when considering stability of magnetization at depth, and different mineral reactions that occurred at different depths in the crust.

Because these properties were measured at ambient *T* and pressure, the Q values shown in Figure 11 are maximal. The ratio is predicted to decrease with increasing temperature to $<T_C$ or T_N of the relevant minerals, because thermal activation reduces remanence-carrying capacity, while simultaneously enhancing thermoviscous magnetization acquisition and, to a lesser degree, weak-field susceptibility. Less than 10% of total samples have a $Q < 0.1$, and nearly 70% are <1. In these samples with increasing depth and *T* in the crust, we expect induced magnetization to dominate the signal.

When applying Q values to predict the strength of magnetic field anomalies, the total magnetization should be considered. The kernel density estimations showing the distribution of Q values by rock type (Figure 10c) indicate that the CG, HP, and UHP groups are generally dominated by a log-normal peak centered at a Q value of 0.5. All have further secondary distributions that show as shoulders on the main peak, such as the case of the asymmetric peak of the HP samples, or a long tail, in the UHP set, that contains a significant population centered around 20. In the HP and UHP areas with very high Q values >5, samples have NRM values >2 A/m and induced magnetization plays a negligible role in their crustal signal. By contrast, more than 50% of MP samples have Q values >1, indicating a stronger NRM component. However, the total magnetizations are very small, with most samples having a maximum total magnetization, where M_i and M_r is aligned in the same direction, <0.2 A/m, so that the total contribution to the crustal signal is very small.

7.4. Susceptibility Versus Density and Calculated Magnetite Content

The density of the samples is primarily controlled by the initial bulk composition of the material prior to metamorphism. Metamorphic reactions can result in an increased density, while maintaining constant molecular weight, with the creation of high-pressure, denser minerals such as garnet, omphacite, and rutile. These reactions can be aided by the presence of a fluid or by deformation, or both. Conversely the mantle peridotite samples, which initially would have the highest densities, have their densities reduced by formation of serpentine by addition of aqueous fluid. In Figure 12, showing susceptibility as a function of density, the MP samples have the lowest densities, due to serpentinization. However, the susceptibility values are low, which indicates little magnetite was created during those reactions, possibly due to the high Mg-content of the protolith olivine. The volume content of magnetite is estimated by k/0.0347 (Clark, 1997) and is plotted on the right axis. The MP samples have a calculated median magnetite content of 0.026%. The CG samples are relatively well clustered in density values and a range of magnetite content from 0.1% to 1.15%. Both HP and UHP groups show a highly skewed distribution with magnetite contents of the HP group from 0.4% to 0.9% and of the UHP group from 0.04% to 0.4%. A caveat to this estimation is that it treats all susceptibility as arising from magnetite. The contribution of rhombohedral oxides to this calculation is minor, because they have susceptibility values much lower than those of magnetite.

7.5. Hysteresis Properties

Hysteresis properties were measured on a VSM at room-T. The ratio of saturation remanent magnetization (Mrs) to saturation magnetization (Ms) is plotted against the ratio of coercivity of remanence (Hcr) to

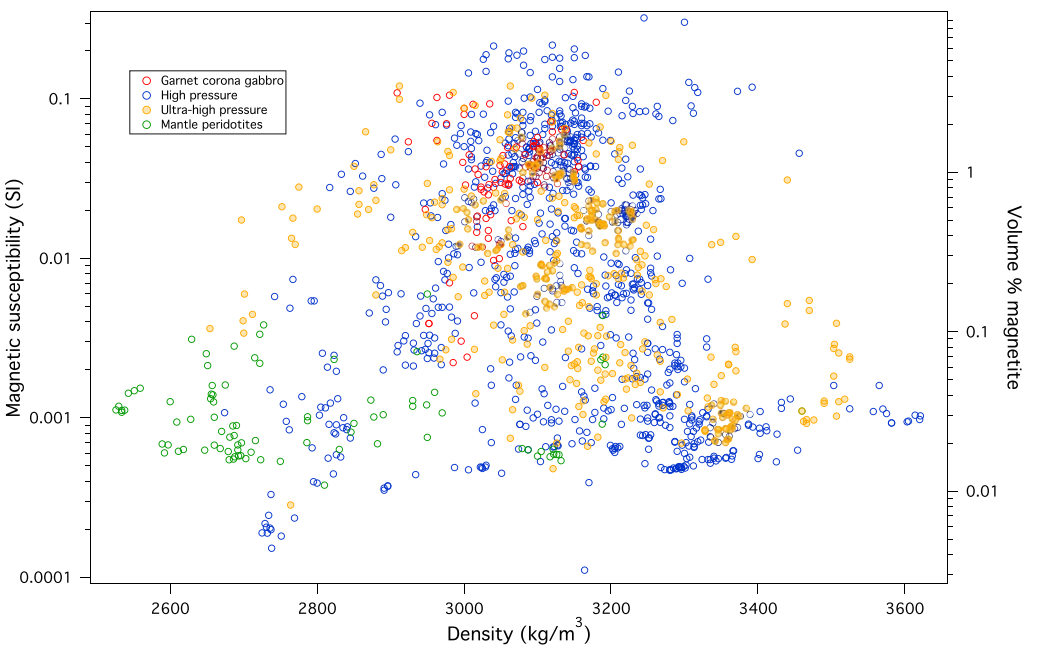

Figure 12. (left axis) Magnetic susceptibility and (right axis) estimated magnetite content as function of density. HP ore samples are excluded, as are three outlying HP and UHP and 1 MP specimen.

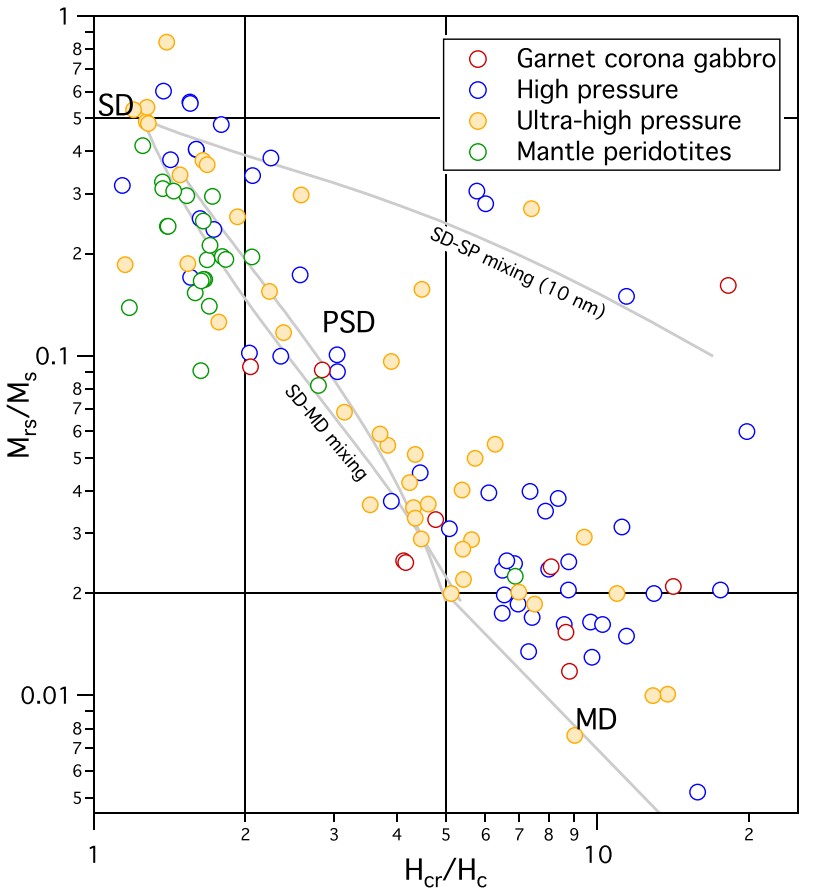

Figure 13. Magnetic hysteresis ratios M_{rs}/M_s versus H_{cr}/H_c in modified Day et al. (1977) plot. Mixing trends and ranges of SD, PSD, and MD properties after Dunlop (2002). With exception of MP samples ratios indicate a wide distribution of inferred domain states. Some HP and UHP samples contain exsolved hematite-ilmenite, which shift values toward, or above ideal SD properties of magnetite.

coercivity (Hc) on a modified Day et al. plot (1977) for 124 samples. This diagram, shown in Figure 13, gives an estimation of the distribution of magnetic domain states from magnetite-bearing rocks. In some samples, these ratios are influenced by coexisting rhombohedral oxides. Mixing lines and theoretical ranges for single-domain (SD), pseudosingle domain (PSD), and multidomain (MD) behavior for magnetite are from Dunlop (2002).

The HP and UHP sample suites show largest variability in hysteresis values that imply a range of domain states from SD to MD, with the data plotting along SD-MD mixing trends. Those samples dominated by MD behavior consistently fall above the MD distribution line calculated using $p = 0.1$, which may reflect the influence of strain fields on domain wall motion, due to exsolution microstructures in magnetite, on domain wall motion.

Both the HP and UHP groups contain a number of specimens with Mrs/Ms values above 0.5, the theoretical maximum for single-domain magnetite particles with dominant shape anisotropy (Stoner & Wohlfarth, 1948). Many of these specimens contain rhombohedral oxides, where ilmenohematites have high Mrs/Ms ratios plotting above the SD region of magnetite. Other samples with high Mrs/Ms values, but below 0.5, represent mixed oxide mineralogy.

The MP and CG suites are more strongly clustered. Some MP samples have high Mrs/Ms and low Hcr/Hc values that approach SD behavior. Because the only oxide phase in the MP samples is magnetite, formed during serpentinization, such behavior likely reflects a mix of SD/PSD magnetite carriers. The CG samples show greater variability, have low Mrs/Ms < 0.03 and plot near the region that delineates ideal MD behavior in

magnetite. This is consistent with the large magnetite grains observed in these samples. The HP, UHP, and CG sample suites contain specimens with high Mrs/Ms (>0.1) and high Hcr/Hc (>5) values, in an area of the Day plot predicted to represent SD-superparamagnetic mixtures (Dunlop, 2002). Because many oxides show evidence of extensive coarsening, the presence of superparamagnetic magnetite would be unusual, except for those samples with ultrafine magnetite in the oxide-silicate symplectite. However, nm size hematite exsolution lamellae in a paramagnetic ilmenite host would have this behavior (Brok et al., 2016; McEnroe et al., 2002).

8. Discussion

Longstanding questions remain concerning the contributions to magnetization of deep-crustal and uppermost-mantle rocks in relation to long-wavelength anomalies. These questions date back to the results from the first analyses of satellite data in the 1970s and 1980s and are pertinent today, with higher resolution data from the new Swarm satellites. Numerous authors have related the formation of metamorphic garnet consuming Fe^{2+}, to the loss of magnetite and assumed that high-grade eclogite-facies rocks are dominantly paramagnetic due to that reaction. Here we have shown that magnetite in some HP and UHP samples can survive these *PT* conditions in part because complete eclogite-facies equilibrium is rarely reached. With the present knowledge that magnetic oxide phases can be preserved in geological settings like the WGR, we can consider their contribution to the magnetic response of the deep crust. The intensity of the remanent and induced response is a function of the size and shape of the magnetic particles, substitution of noniron cations in solid solutions, and thermal history, as well as present-day *T* conditions at depth.

The presence of exsolution microstructures has a profound effect on the magnetic behavior of both ilmenite-hematite, and magnetite-bearing rocks. Intermediate compositions of the ilmenite-hematite solid solution (ilm50–70) have low Néel *T*s from 200°C for the Fe richer compositions to close to R*T* and slightly Ti-richer compositions will be paramagnetic. However, exsolution into chemical domains that approach pure Fe_2O_3 and Fe_2TiO_3 is the origin of strong NRM due to magnetic ordering at phase interfaces. This exsolution occurs at high temperatures, and is stable to relatively high temperatures (near their respective T_N). The strength of the NRM is a function of the amount of oxide, microstructures and lattice-preferred orientations (Robinson et al., 2013). The low susceptibility of ilmenite-hematite$_{ss}$ (<0.005 SI), results in low M*i* and high Q values. From the perspective of anomalies, this means that a significant component will be in the direction of the "permanent magnetization." Based on extensive petrographic observations, these minerals appear to be less involved in garnet formation than is magnetite in the WGR.

The presence of microstructures in magnetite has significant effects on magnetic properties, due to its role in controlling particle size and shape. The oxide grain size in the CG, HP, and UHP samples is generally large (10s to 100s of μm), which, if single-phase, would have MD behavior. MD magnetite is highly responsive to weak fields, and yields strong induced magnetization and subordinate viscous remanent magnetization (VRM) in the direction of the present-day Earth field. With increased temperature, MD magnetite is unlikely to retain primary NRMs over geological times, but will contribute a VRM. The magnetite grains observed in the WGR gabbro samples are subdivided by oxy-exsolution of ilmenite and subsolvus exsolution of spinel, which reduces the grain size and may enhance some remanence-carrying capacity. The magnesium-aluminum spinel/magnetite solvus occurs between 900 and 1,000°C (Mattioli & Wood, 1988), suggesting that this microstructure likely is preserved under metamorphic conditions. The conditions that control the oxidation exsolution of ilmenite from titanomagnetite are less well constrained, as oxygen fugacity plays a controlling role and thermodynamic models and laboratory experiments indicate that it can occur at temperatures at least as low as 550°C. The oxy-exsolution structures may not be stable at metamorphic temperatures, in which case titanomagnetite would have a Curie temperature below that of end-member magnetite with reduced susceptibility and remanence. Depending on the exact conditions of oxidation, in the HP and UHP rocks at high T, ilmenite lamellae in magnetite may be resorbed back into solid solution with only one phase at high T and P. The implications of this interpretation are that this material would be paramagnetic at significant depths in the crust and with cooling upon exhumation; ilmenite lamellae would exsolve. The interstitial subparticles are depleted in Ti, approaching end-member magnetite, and obtain a magnetization during this cooling process. Here, the role of fine-grained magnetite produced in the very-

fine silicate symplectite formed (Figure 8) during exhumation could be an important stable remanence carrier.

An equally possible interpretation is that the prograde growth of garnet rims on original titanomagnetite grains extracted FeO from the oxide, thus driving the residual composition from original titanomagnetite to a mixture of Ti-poor magnetite and ilmenite lamellae. Absence of strong and transient episodes of reduced oxygen fugacity, such that a two-phase "oxy-exsolved" mixture could not be resorbed during exhumation.

Other than composition, the dominating factor on the stability of magnetization is temperature. The main influencing factors in magnetization are the depth to the Curie isotherm (for magnetite), or Néel isotherm for the rhombohedral oxides. At temperatures above these values, 580°C for magnetite and 675°C for pure hematite (assuming no pressure effect), the minerals become paramagnetic, losing both induced and remanent magnetic responses, and will not contribute to long-wavelength anomalies. These responses depend on heat flow in the region. Magnetization in cold cratonic crust will be maintained to deeper levels than in areas of high heat flow. Variations in crustal thickness, and radiogenic heat generation may influence heat flow, in turn having an effect on depth of the T_C/T_N isotherms.

In some cratonic areas with normal heat flow, the crust and parts of the upper mantle can contribute to magnetic anomalies. Saltus and Hudson (2007) and Ferré et al. (2014) have proposed that significant contribution could come from mantle rocks that are cooler than the Curie *T*. Further Ferré et al. (2014) propose that mantle rocks can make a significant contribution to the total lithospheric magnetic signal. The important question here is what is the stable in situ spinel phase in mantle rocks. From our view magnetite would be somewhat unusual, and observations of the magnetic carriers in the MP samples suggest that these contain little primary magnetite, and what weak magnetization contributed by these mantle rocks at the surface derives from later, low-temperature serpentinization. However, too limited magnetic property data exists to address this question, or the effects of deserpentization on recycled serpentized oceanic crust.

Other important factors are the potential effects of pressure on the Curie/Néel temperatures, presently very poorly known. Chemical and experimental work on the ilmenite-hematite system (McEnroe et al., 2004, 2008) at 10 kbar, and the effect of pressure on the Fe-Ti ordering temperature in that system (Harrison et al., 2006) implies that increased pressure has the effect of raising the consolute temperature and widening the ilmenite-hematite solvus. If correct, the lamellae within exsolved grains would remain stable to higher *Ts* at higher pressures. If not, then exsolved grains would lose their lamellar magnetizations at lower temperatures due to reabsorption of lamellae.

Experimental work on magnetite indicates a very minor increase in Curie *T* with pressure of approximately 2°C/kb or 20°C per10 kb, with a lesser effect in samples containing Ti in solid solution (Schult, 1970). However, the effects of Al substitution or of related exsolution lamellae are unknown.

The variety of oxide minerals and microstructures observed in these rocks leads to very different behaviors in the Earth's field. The response measured by aerial surveys is the vector sum of the induced and remanent magnetization, which in this study is unconstrained. Calculations in section 2 (from Parker, 2003) indicate that the minimum magnetization for a 15 km thick crust that accounts for the observed field values in the WGR is 0.42 A/m, assuming a linear structure that is consistent with qualitative observations of regional field features. Without the inferred linear geometry, this minimum is 0.3 A/m. These estimates require specific crustal magnetization geometries unlikely to occur in nature: the uniform direction of induced magnetization and VRM is certainly not similar to the varying geometry that underlies the calculation of a minimum magnetization. The minimum magnetization is a strict lower limit, and more realistic values take into account the uniform direction of induced magnetization and VRM or scatter in NRM directions would be higher. Statistical modeling of the effect of realistic nonuniformity of NRM directions is beyond the scope of this study.

While this data set is not fully representative of the Western Gneiss Region as a whole, we can use these minimum values to generalize on the contribution of the mafic and ultramafic rocks to the total magnetic field. The magnetization of the MP samples falls below both estimates for nearly all samples: 83% of samples have an absolute maximum magnetization (where NRM is aligned with inducing field) below 0.3 A/m, and 90% fall below 0.42 A/m calculated for the more realistic spatial geometry. Therefore, the MP group contributes little to the field associated with the WGR. By contrast, the minimum magnetization of the CG

samples (calculated as the absolute difference between in situ induced magnetization and measured NRM) lies above 0.3 A/m for over 80% of the samples, and above 0.42 A/m for 75%. Therefore, the CG samples contribute to the crustal signal, largely through their induced component, as Figure 10d indicates that this component is dominant in nearly all CG samples. The petrology of these rocks with large MD magnetite grains may indicate that there could be a favorable pressure and temperature conditions for the formation of magnetite in these bulk compositions.

A similar calculation for the HP and UHP samples indicate that a significant proportion of the total sample set have minimum magnetizations greater than that required to generate the observed field. Approximately 37% of the UHP, and 32% of HP samples (excluding ores) have minimum magnetizations above 0.42 A/m and also have Q values < 0.5, indicating that NRM plays a minor role in controlling the total magnetization. If 0.3 A/m is considered a reasonable lower limit, 30% of both data sets exceed this value, irrespective of NRM direction. With the addition of NRM directional information, the intensity of the induced magnetization-dominated sample set would increase above the minimum calculated here. Furthermore, this calculation completely discounts those samples dominated by NRM: with any degree of regional coherence to the NRM directions, such samples would contribute to the regional field to potentially reinforce, or reduce that generated by the induced samples. Because petrological and structural studies of the mafic bodies in the WGR, (area of 28,000 km^2) show different cooling rates, different oxide mineralogy, and relatively low-T deformation of the enclosing rocks, these combined features on a regional scale would result in a less-unified vector that would lowers the remanent contribution to the magnetic signal.

What is surprising is that numerous the HP and UHP rocks retain magnetite and rhombohedral oxides. In some studies worldwide, significant portions of deep-crustal rocks are reported to be paramagnetic. Here we find preserved magnetic oxides in rocks exposed to ultradeep conditions, where limited access to catalyzing fluids or deformation, hampered progress toward high-P assemblages. It is possible that there is more of a magnetic contribution than earlier assumed for deep-crustal rocks, provided the geotherm is appropriate. Compared to global-scale studies, the bulk susceptibility values of 0.04 SI, which provide a general upper bound to the magnetic susceptibilities, are significantly higher than what is measured in our data set, except for the corona gabbro (CG) samples with a mean, susceptibility of 0.04 SI. Using an induced magnetization assumption, this value has been successful in modeling more than 95% of the satellite observations (Thébault et al., 2010). Therefore, the question still remains open, can we account for the magnetization that is used in current global-scale models of satellite data for continental rocks, or are the model assumptions incomplete?

9. A Long Trip Down and Back Up Again

The rocks reported on here, with their varied trips to depth in a subduction and continental collision zone, are not fully representative of rock types creating magnetic anomalies in the deep crust and upper mantle, however they have properties representative of some residing deep in the crust. The rocks discussed here are dominantly mafic and ultramafic rocks that make up only a portion of rocks in the Western Gneiss Region, where felsic gneisses, not included in the study, are predominant. The mafic and ultramafic histories can be thought of in three stages: (1) The initial histories involving the magnetic oxides of the original igneous rocks. (2) The mineralogical transformations of the magnetic oxides produced during subduction to high or ultrahigh pressure and high temperature. (3) The mineralogical transformations of the magnetic oxides during pressure release during exhumation and during cooling from high temperature.

These rocks reached the end of a major cycle by eventually reaching the Earth's surface. By contrast, rocks presently in the deep crust and upper mantle remained at depth and at relatively high temperature for an untold length of time. Therefore, these did not undergo any mineralogical changes that could be expected in the final stages of exhumation and cooling, and with magnetic properties only held at high temperatures and pressures expected at depth. The mineralogical changes can be understood with reasonable certainty, based on applicable phase diagrams, but with uncertainties coupled to the kinetics of chemical reactions related to growth or resorption of exsolution lamellae. By contrast there is too little data on the expected effects of pressure on the Curie or Néel temperatures, and intensities of magnetization of magnetic oxides.

In process of studying this collection of mafic and ultramafic rocks, we made certain observations and arrived at questions that merit further detailed work: (1) Are there certain P-*T* or fluid conditions that favor

growth, preservation, or destruction of magnetite? (2) What are the conditions that produce fine magnetite-silicate symplectites, commonly between coarse magnetite and garnet? (3) At what temperature in this pressure regime would earlier oxidation-exsolution lamellae of ilmenite be resorbed into magnetite? The Ti added to the magnetite would lower the Curie *T*. (4) Hemoilmenite and ilmenohematite are better preserved in these varying metamorphic histories than is magnetite. Why are these apparently better preserved and does this enhance the remanent contribution? The problems investigated here, especially Curie and Néel temperatures, will not be solved without a broad, creative and expensive program of high-pressure magnetic experiments at high temperatures.

Acknowledgments
This research was funded by Norwegian Research Council grant 222666. Laurie Brown graciously measured some samples and allowed access to her 2G cryogenic magnetometer, and A. R. McEnroe for help with susceptibility measurements. Clemens Reimann kindly provided help with initial statistical analyses. This research is a spin-off of a WGR paleomagnetic project funded by an NSF international postdoctoral fellowship program to S. McEnroe in1994–1995, where data were too diverse to allow for firm results. However, that research provided valuable data used here to study crustal magnetism. We thank David Clark and Rick Saltus for their excellent and constructive reviews that improved this manuscript.

References

Airo, M., & Säävuori, H. (2013). *Petrophysical characteristics of Finnish bedrock – Concise handbook on the physical parameters of bedrock* (Report of Investigation 205, 33 pp.). Espoo, Finland: Geological Survey of Finland.

Ashwal, L. D,. Leo, G. W., Robinson, P., Zartman, R. E., & Hall, D. J. (1979). The Belchertown quartz monzodiorite pluton, West-central Massachusetts: A syntectonic Acadian intrusion. *American Journal of Science*, *279*(8), 936–969.

Auglænd, S. (2017). *Geophysical expression and structural setting of the Averøy eclogite*, (MSc thesis). Trondheim, Norway: NTNU.

Auglænd, S., Robinson, P., McEnroe, S. A., Terry, M. P., Daczko, N., Krogh, T. E., Kamo, S. L., & Hollocher, K. (2017). Tectonostratigraphy, structure and petrology of the Averøy layered eclogite and relations to the Nordøyane UHP domain, W Norway. 12th International Eclogite Conference, Åre, Sweden.

Austreim, H. (1987). Eclogitization of lower crustal granulites by fluid migration through shear zones. *Earth and Planetary Science Letters*, *81*, 221–232.

Austreim, H. (2013). Fluid and deformation induced metamorphic processes around Moho beneath continental collision zones: Examples from the exposed root zone of the Caledonian mountain belt, West Norway. *Tectonophysics*, *609*, 620–635. https://doi.org/10.1016/jtecto.2013.08.030

Beckman, V., Möller, C., Söderlund, U., Corfu, F., Pallon, J., & Chamberlain, K. (2014). Metamorphic zircon formation at the transition from gabbro to eclogite in Trollheimen-Surnadalen, Norwegian Caledonides. In F. Corfu, D. Gasser, & D. M. Chew (Eds.) *New perspectives on the Caledonides of Scandinavia and related areas* (Vol. 390, pp. 403–424). London: Geological Society.

Blakely, R. J., Brocher, T. M., & Wells, R. E. (2005). Subduction-zone magnetic anomalies and implications for hydrated forearc mantle. *Geology*, *33*, 445–448. https://doi.org/10.1130/G21447.1

Brok, E., Frandsen, C., Lefmann, K., McEnroe, S. A., Robinson, P., Burton, B. P., et al. (2017). Spin orientation in solid solution hematite-ilmenite. *American Mineralogist*, *102*, 1234–1243. http://dx.doi.org/10.2138/am-2017–5792CCBY

Brown, L. L., & McEnroe, S. A. (2008). Magnetic properties of Anorthosites: A forgotten source for planetary magnetic anomalies? *Geophysical Research Letters*, *35*, L02305. https://doi.org/10.1029/2007GL032522

Brown, L. L., Webber, J., Williams, M. J., Regan, S., & Seaman, S. (2014). Magnetism of the lower crust: Observations from the Chipman Domain, Athabasca Granulite Terrain, northern Canada. *Tectonophysics*, *624–625*, 66–74.

Brueckner, H. K., Carswell, D. A., Griffin, W. L., Medaris, L. G., Jr., van Roermund, H. L. M., & Cuthbert, S. J. (2010). The mantle and crustal evolution of two garnet peridotite suites from the Western Gneiss Region, Norwegian Caledonides: An isotopic investigation. *Lithos*, *117*(1–4), 1–19. https://doi.org/10.1016/j.lithos.2010.01.011

Butler, J. P., Beaumont, C., & Jamieson, R. A. (2015). Paradigm lost: Buoyancy thwarted by the strength of the Western Gneiss Region (ultra) high-pressure terrane, Norway. *Lithosphere*, *7*(4), 379–407.

Butler, J. P., Jamieson, R. A., Steenkamp, H. M., & Robinson, P. (2012). Discovery of coesite-eclogite from the Nordøyane UHP domain, Western Gneiss Region, Norway: Field relations, metamorphic history and tectonic significance. *Journal of Metamorphic Geology*, *31*, 147–163. https://doi.org/10.1111/jmg.12004

Carswell, D. A. (1973). Garnet pyroxenite lens within the Ugelvik layered garnet peridotite. *Earth and Planetary Science Letters*, *20*, 249–260.

Carswell, D. A., Tucker, R. D., O'Brien, P. J., & Krogh, T. E. (2003). Coesite microinclusions and the U-Pb age of zircons from the Hareidland Eclogite in the Western Gneiss Region of Norway. *Lithos*, *67*, 181–190.

Clark, D. A. (1997). Magnetic petrophysics, and magnetic petrology: Aids to geological interpretation of magnetic surveys. *Journal of Australian Geology and Geophysics*, *17*, 83–103.

Clark, D. A. (1999). Magnetic petrology of igneous intrusions: Implications for exploration and magnetic interpretation. *Exploration Geophysics*, *30*(2), 5–26.

Corfu, F., Austreim, H., & Ganzhorn, A.-C. (2014). Localized granulite and eclogite-facies metamorphism at Flatraket and Kråkeneset, Western Gneiss Region: U-Pb data and tectonic implications. In F. Corfu, D. Gasser, & D. M. Chew (Eds.), *New perspectives on the Caledonides of Scandinavia and related areas* (Vol. 390, pp. 425–442). London: Geological Society.

Cuthbert, S. J. (1985). *Petrology and tectonic setting of relatively low temperature eclogites and related rocks in the Dalsfjord area, Sunnfjord, West Norway* (PhD thesis). Sheffield, UK: University of Sheffield.

Day, R., Fuller, M., & Schmidt, V. A. (1977). Hysteresis properties of titanomagnetites: Grain-size and compositional dependence. *Physics of the Earth and Planetary Interiors*, *13*(4), 260–267. https://doi.org/10.1016/0031-9201(77)90108-X

Dobrzhinetskaya, L. F., Eide, E. A., Larsen, R. B., Sturt, B. A., Trønnes, R. G., Smith, D. C., et al. (1995). Microdiamond in high-grade metamorphic rocks of the Western Gneiss Region, Norway. *Geology*, *23*, 597–600.

Dunlop, D. J. (2002). Theory and application of the Day plot (Mrs/Ms versus Hcr/Hc). 1: Theoretical curves and tests using titanomagnetite data. *Journal of Geophysical Research*, *107*(B3), 2056. https://doi.org/10.1029/2001JB000486

Dunlop, D. J., Özdemir, Ö., & Costanzo-Alvarez, V. (2010). Magnetic properties of rocks of the Kapuskasing uplift (Ontario, Canada) and origin of long-wavelength magnetic anomalies. *Geophysical Journal International*, *183*(2), 645–658.

Dyar, D. M., McEnroe, S. A., Murad, E., Brown, L. L., & Schiellerup, H. (2004). The relationship between exsolution and magnetic properties in hemo-ilmenite: Insights from Mössbauer spectroscopy. *Geophysical Research Letters*, *31*, L04608. https://doi.org/10.1029/2003GL019076

Dyment, J., Lesur, V., Hamoudi, M., Choi, Y., Thebault, E., & Catalan, M. (2016). World Digital Magnetic Anomaly Map version 2.0. Abstract GP13B-1310 presented at the 2015 AGU Fall Meeting, San Francisco, Calif. Retrieved from http://www.wdmam.org

Ferré, E. C., Friedman, S. A., Martín-Hernández, F., Feinberg, J. M., Till, J. L., Ionov, D. A., et al. (2014). Eight good reasons why the uppermost mantle could be magnetic. *Tectonophysics*, *624–625*, 3–14.

Hacker, B. R., Andersen T. B., Kylander-Clark, A. R. C., Johnston, S., Peterman, E., Walsh, E. O., & Young, D. (2010). High-temperature deformation during continental-margin subduction and exhumation: The ultrahigh-pressure Western Gneiss Region of Norway. *Tectonphysics*, *480*, 149–171.

Harrison, R. J., Stone, H. J., & Redfern, S. A. T. (2006). Pressure dependence of Fe-Ti order in the ilmenite-hematite solid solution: Implications for the origin of lower crustal magnetization. *Physics of the Earth and Planetary Interiors*, *154*(3–4), 266–275.

Hemant, K., & Maus, S. (2005). Geological modeling of the new CHAMP magnetic anomaly maps using a geographical information system technique. *Journal of Geophysical Research*, *110*(B12). https://doi.org/10.1029/2005JB003837

Kelso, P. R., Banerjee, S. K., & Teyssier, C. (1993). Rock magnetic properties of the Arunta Block, Central Australia, and their implication for the interpretation of long-wavelength magnetic anomalies. *Journal of Geophysical Research*, *98*(B9), 15987–15999.

Korneliussen, A., McLimanns, R., Braathen, A., Erambert, M., Lutro, O., & Ragnhildstveit, J. (2000). Rutile in eclogites as a mineral resource in the Sunnfjord Region, W. Norway. *Norges geologiske undersøkelse Bulletin*, *436*, 39–47.

Krogh, T. E., Kamo, S. L., Robinson, P., Terry, M. P., & Kwok, K. (2011). U-Pb zircon geochronology of eclogites from the Scandian Orogen, northern Western Gneiss Region, Norway: 14–20 million years between eclogite crystallization and return to amphibolite-facies conditions. *Canadian Journal of Earth Sciences*, *48*(2), 441–472.

Liu, Q., Frost, B. R., Hongcai, W., Zheng, J., & Zeng, Q. (2012). Magnetic petrology of high Fe-Ti eclogites from the CCSD main hole: Implications for subduction-zone magnetism. *Journal of Geophysical Research*, *117*, B07102. https://doi.org/10.1029/2011JB008621

Lowe, D. A. J., Parker, R. L., Purucker, M. E., & Constable, C. G. (2001). Estimating the crustal power spectrum from vector Magsat data. *Journal of Geophysical Research*, *106*, 8589–8598. https://doi.org/10.1029/2000JB900437

Lund, M. G., & Austrheim, H. (2003). High-pressure metamorphism and deep-crustal seismicity: Evidence from contemporaneous formation of pseudotachylytes and eclogite facies coronas. *Tectonophysics*, *372*, 59–83.

Mattioli, G. S., & Wood, B. J. (1988). Magnetite activities across the $MgAl_2O_4$-Fe_3O_4 spinel join, with application to thermobarometric estimates of upper mantle oxygen fugacity. *Contributions to Mineralogy and Petrology*, *98*(2), 148–162. https://doi.org/10.1007/BF00402108

Maus, S., Rother, M., Hemant, K., Stolle, C., Lühr, H., Kuvshinov, A., & Olsen, N. (2006). Earth's lithospheric magnetic field determined to spherical harmonic degree 90 from CHAMP satellite measurements. *Geophysical Journal International*, *164*, 319–330. https://doi.org/10.1111/j.1365-246X.2005.02833.x

McCammon, C., McEnroe, S. A., Robinson, P., Fabian, K., & Burton, B. P. (2009). Mössbauer spectroscopy used to quantify natural lamellar remanent magnetization in single-grains of ilmeno-hematite. *Earth and Planetary Science Letters*, *288*(1–2), 268–278.

McEnroe, S. A., & Brown, L. L. (2000). A closer look at remanence-dominated aeromagnetic anomalies: Rock magnetic properties and magnetic mineralogy of the Russell Belt microcline-sillimanite gneiss, northwest Adirondack Mountains, New York. *Journal of Geophysical Research*, *105*(B7), 16437–16456.

McEnroe, S. A., Brown, L. L., & Robinson, P. (2009a). Remanent and induced magnetic anomalies over a layered intrusion: Effects from crystal fractionation and magma recharge. *Tectonophysics*, *478*(1), 119–134. https://doi.org/10.1016/j.tecto.2008

McEnroe, S., Fabian, K., Robinson, P., Gaina, C., & Brown, L. (2009b). Crustal magnetism, lamellar magnetism and rocks that remember. *Elements*, *5*(4), 241–246. https://doi.org/10.2113/gselements.5.4.241

McEnroe, S. A., Hemant, K., & Skilbrei, J. R. (2006). Magnetic contributions of minerals at the surface and at depth in the crust: Comparing anomaly maps from aeromagnetic and satellite data from Scandinavia. In *Proceeding from First International SWARM Meeting, 3–5 May, 2006 Nantes, France*. Noordwijk, the Netherlands: ESA WPP-261 European Space Agency Publications.

McEnroe, S. A., Langenhorst, F., Robinson, P., Bromiley, G. D., & Cliff, S. J. S. (2004). What is magnetic in the lower crust? *Earth and Planetary Science Letters*, *226*(1–2), 175–192.

McEnroe, S. A., Robinson, P., Langenhorst, F., Frandsen, C., Terry, M. P., & Boffa Ballaran, T. (2007). Magnetization of exsolution intergrowths of hematite and ilmenite: Mineral chemistry, phase relations, and magnetic properties of hemo-ilmenite ores with micron- to nanometer-scale lamellae from Allard lake, Quebec. *Journal of Geophysical Research*, *112*, B10103. https://doi.org/10.1029/2007JB004973

McEnroe, S. A., Robinson, P., Miyajima, F., Langenhorst, & Terry, M. P. (2008). *Comparative TEM study of exsolution lamellae in hemo-ilmenite in igneous rock emplaced at 5 kbar and gabbro rapidly uplifted after eclogite facies metamorphism key to contrasting magnetizations* (annual report). Bayreuth, Germany: Bayerisches Geoinstitut, University of Bayreuth.

McEnroe, S. A., Harrison, R., Robinson, P., Golla, U., & Jercinovic, M. J. (2001a). The effect of fine-scale microstructures in titanohematite on the acquisition and stability of NRM in granulite facies metamorphic rocks from southwest Sweden: Implications for crustal magnetism. *Journal of Geophysical Research*, *106*, 30523–30546.

McEnroe, S. A., Robinson, P., & Panish, P. (2001b). Aeromagnetic anomalies, magnetic petrology and rock magnetism of hemo-ilmenite- and magnetite-rich cumulates from the Sokndal Region, South Rogaland, Norway. *American Mineralogist*, *86*(11–12), 1447–1468.

McEnroe, S. A., Robinson, P., & Panish, P. T. (1996). *Rock magnetic properties, oxide mineralogy, and mineral chemistry in relation to aeromagnetic interpretation and search for ilmenite reserves* (Geological Survey of Norway Report 96.060). Trondheim, Norway: Geological Survey of Norway.

McEnroe, S. A., Robinson, P., Rønning, S., & Panish, P. T. (1998). Significance of high-coercivity rhombohedral oxides and fine-grained magnetite for the origin of strong remanence dominated aeromagnetic anomalies, South Rogaland, Norway. *Geologica Carpathica*, *49*, 223–224.

Michels, A., McEnroe, S., Church, N., & Pastore, Z. (2015). Geophysical model of the Leka Ophiolite complex. In *26th IUGG* (22.06-02.07). IUGG: Prague, Czech Republic.

Möller, C. (1998). Decompressed eclogites in the Sveconorwegian (-Grenvillian) orogen of SW Sweden: Petrology and tectonic implications. *Journal of Metamorphic Geology*, *16*(5), 641–656. https://doi.org/10.1111/j.1525-1314.1998.00160.x

Mooney, W. D. (2007). Crust and lithosphere-global crustal structure. In M. Kono (Ed.), *Seismology and the structure of the earth, Treatise on Geophysics* (Chap. 11, Vol. 1, pp. 361–399). Amsterdam, the Netherlands: Elsevier.

Olsen, N., H. Lühr, H., Sabaka, T. J., Mandea, M., Rother, M., Toffner-Clausen, L., & Choi, S. (2006). CHAOS-a model of the Earth's magnetic field derived from CHAMP, Orsted, and SAC-C magnetic satellite data. *Geophysical Journal International*, *166*. https://doi.org/10.1111/j.1365-246X.2006.02959.x

Olsen, N., Ravat, D., Finlay, C. C., & Kother, L. K. (2017). LCS-1: A high-resolution global model of the lithospheric magnetic field derived from CHAMP and Swarm satellite observations. *Geophysical Journal International*, *211*(3), 1461–1477.

Parker, R. L. (2003). Ideal bodies for Mars magnetics. *Journal of Geophysical Research*, *108*(E1), 5006. https://doi.org/10.1029/2001JE001760

Pilkington, M., & Percival, J. A. (1999). Crustal magnetization and long-wavelength aeromagnetic anomalies of the Minto block, Quebec. *Journal of Geophysical Research*, *104*, 7513–7526.

Pilkington, M., & Percival, J. A. (2001). Relating crustal magnetization and satellite-altitude magnetic anomalies in the Ungava peninsula, northern Quebec, Canada. *Earth and Planetary Science Letters*, *194*(1–2), 127–133.

Purucker, M. E., & Clark, D. A. (2011). Mapping and interpretation of the lithospheric magnetic field. In M. Mandea & M. Korte (Eds.), *Geomagnetic observations and models, IAGA special Sopron book series* (Vol. 5, pp. 311–337). Dordrecht, the Netherlands: Springer.
Regan, R. D., Cain, J. C., & Davis, W. M. (1975). A global magnetic anomaly map. *Journal of Geophysical Research*, *80*, 794–802.
Reynolds, R. L., Rosenbaum, J. G., Hudson, M. R., & Fishman, N. S. (1990). Rock magnetism, the distribution of magnetic minerals in the Earth's crust, and aeromagnetic anomalies. *United States Geological Survey Bulletin*, *1924*, 24–45.
Robinson, P. (1991). The eye of the petrographer, the mind of the petrologist. *American Mineralogist*, *76*, 761–790.
Robinson, P., Fabian, K., McEnroe, S. A., & Heidelbach, F. (2013). Influence of lattice-preferred orientation with respect to magnetizing field on intensity of remanent magnetization in polycrystalline hemo-ilmenite. *Geophysical Journal International*, *192*(2), 514–536. https://doi.org/10.1093/gji/ggs046
Robinson, P., Harrison, R. J., McEnroe, S. A., & Hargraves, R. (2002). Lamellar magnetism in the hematite-ilmenite series as an explanation for strong remanent magnetization. *Nature*, *418*, 517–520.
Robinson, P., Harrison, R. J., McEnroe, S. A., & Hargraves, R. (2004). Nature and origin of lamellar magnetism in the hematite-ilmenite series. *American Mineralogist*, *89*, 725–747.
Robinson, P., McEnroe, S. A., Miyajima, N., Fabian, K., & Church, N. (2016). Remanent magnetization, magnetic coupling, and interface ionic configurations of intergrown rhombohedral and cubic Fe-Ti oxides: A short survey. *American Mineralogist*, *101*(3), 518–530. https://doi.org/10.2138/am-2016–5519
Robinson, P., Roberts, D., Solli, A., & Gee, D. G. (2014). A major synmetamorphic Early Devonian thrust and extensional fault system in the Mid Norway Caledonides. In F. Corfu, D. Gasser, & D. M. Chew (Eds.), *New perspectives on the Caledonides of Scandinavia and related areas* (Vol. 390, pp. 241–270). London: Geological Society.
Root, D. B., Hacker, B. R., Gans, P. B., Ducea, M. N., Eide, E. A., & Mosenfelder, J. L. (2005). Discrete ultrahigh-pressure domains in the Western Gneiss Region, Norway: Implications for formation and exhumation. *Journal of Metamorphic Geology*, *23*(1), 45–61.
Sabaka, T., Olsen, N. & Purucker, M. E. (2004). Extending comprehensive models of the earth's magnetic field with Oersted and CHAMP data. *Geophysical Journal International*, *159*, 521–547. https://doi.org/10.1111/j.1365-246X.2004.02421.x
Saltus, R. W., & Hudson, T. L. (2007). Regional magnetic anomalies, crustal strength, and the location of the northern Cordilleran fold-and-thrust belt. *Geology*, *35*(6), 567–570. https://doi.org/10.1130/G23470A.1
Scambelluri, M., Pettke, T., & van Roermund, H. (2008). Majoritic garnets monitor deep subduction fluid flow and mantle dynamics. *Geology*, *36*, 59–62.
Scambelluri, M., van Roermund, H., & Pettke, T. (2010). Mantle wedge peridotites: Fossil reservoirs of deep Subduction processes inferences from high and ultrahigh pressure rocks from Bardane (Western Norway) and Ulten (Italian Alps). *Lithos*, *120*(1–2), 186–201.
Schlinger, C. M. (1985). Magnetization of lower crust and interpretation of regional magnetic anomalies: Example from Lofoten and Vesteralen, Norway. *Journal of Geophysical Research*, *90*(B13), 11484–11504.
Schmidt, P. W., McEnroe, S. A., Clark, D. A., & Robinson, P. (2007). Magnetic properties and potential field modeling of the Peculiar Knob metamorphosed iron formation, South Australia: An analog for the source of the intense Martian magnetic anomalies? *Journal of Geophysical Research*, *112*, B03102. https://doi.org/10.1029/2006JB004495
Schult, A. (1970). Effect of pressure on the Curie temperature of titanomagnetites [(1 − x)· Fe3O4 − x· TiFe2O4]. *Earth and Planetary Science Letters*, *10*(1), 81–86. https://doi.org/10.1016/0012-821X(70)90067-1
Shive, P. N., Blakeley, R. J., Frost, B. R., & Fountain, D. M. (1992). Magnetic properties of the lower continental crust. In D. M. Fountain, R. Arculus, & R. W. Kay (Eds.), *Continental lower crust* (pp. 145–177). New York, NY: Elsevier.
Smith, D. C. (1984). Coesite in clinopyroxene in the Caledonides and its implications for geodynamics. *Nature*, *310*(5979), 641–644.
Spengler, D., Brueckner, H. K., Van Roermund, H. L. M., & Drury, M. R. (2009). Long-lived, cold continental subduction of Baltica towards 200 km depth. *Earth and Planetary Science Letters*, *281*, 27–35.
Stoner, E. C., & Wohlfarth, E. P. (1948). A mechanism of magnetic hysteresis in heterogeneous alloys. *Philosophical Transactions of the Royal Society of London A*, *240*(826), 599–642. https://doi.org/10.1098/rsta.1948.0007
Strada, E., Talarico, F., & Florindo, F. (2006). Magnetic petrology of variably retrogressed eclogites and amphibolites: A case study from the Hercynian basement of northern Sardinia (Italy). *Journal of Geophysical Research*, *111*, B12S26. https://doi.org/10.1029/2006JB004574
Strømøy, E. K. (2014). *Characterisation of the magnetic mineralogy, properties and magnetic anomaly responses of two garnetiferous peridotite bodies in the WGR, Otrøya: Ground magnetic surveying, sampling, magnetic characterisation and 2D modelling* (MSc thesis). Trondheim, Norway: NTNU.
Terry, M. P. (2010). The potential for determining the PT evolution of rocks at UHP conditions using Cr in garnet- and spinel-bearing Kvalvika peridotite, Western Gneiss Region, Norway. *Geological Society of America Abstracts With Programs*, *42*, 49.
Terry, M. P., & Heidelbach, F. (2004). Superplasticity in garnet from eclogite facies shear zones in the Haram Gabbro, Haramsøya, Norway. *Geology*, *32*(4), 281–284.
Terry, M. P., & Heidelbach, F. (2006). Deformation-enhanced metamorphic reactions and the rheology of high-pressure shear zones, Western Gneiss Region, Norway. *Journal of Metamorphic Geology*, *24*(1), 3–18.
Terry, M. P., Heidelbach, F., Couvy, H., Bromiley, G. D., & Krogh, T. E. (2005). History from the Kvalvika mantle peridotite, Norway: Implications for crust-mantle interactions, and conditions and timing for olivine c-slip during continental subduction. Geological Society of America. *Abstracts With Programs*, *37*, 389.
Terry, M. P., & Robinson, P. (2003). Evolution of amphibolite-facies structural features and boundary conditions for deformation during exhumation of HP and UHP rocks, Nordøyane, Western Gneiss Region, Norway. *Tectonics*, *22*(4), 1036–1059.
Terry, M. P., Robinson, P., Carswell, D. A., & Gasparik, T. (1999). Evidence for a Proterozoic mantle plume and a thermotectonic model for exhumation of garnet peridotites, Western Gneiss Region, Norway. *Eos Transactions American Geophysical Union*, *89*, S359–360.
Terry, M. P., Robinson, P., Krogh, T., & Hollocher, K. (2008). Day 9: Geology of Haramsøy, Flemsøy and Lepsøy. In P. Robinson et al. (Eds.), *Guidebook: A tectonostratigraphic transect across the central Scandinavian Caledonides, 33rd International Geological Congress*. Oslo, Norway (pp. 1–24).
Terry, M. P., Robinson, P., & Ravna, E. J. K. (2000). Kyanite eclogite thermobarometry and evidence for thrusting of UHP over HP metamorphic rocks, Nordøyane, Western Gneiss Region, Norway. *American Mineralogist*, *85*(11–12), 1637–1650.
Thébault, E., Purucker, M., Whaler, K. A., Langlais, B., & Sabaka, T. J. (2010). The magnetic field of the Earth's lithosphere. *Space Science Reviews*, *155*(1–4), 95–127. https://doi.org/10.1007/s11214-010-9667
Tørudbakken, B. O. (1982). *En geologiske undersøkelse av nordre Trollheimen ved Surnadal, med hovedvekt på sammenhengen mellow strukterer, metamorphose og aldersforhold* (Real thesis). Oslo, Norway: Universitetet i Oslo.

Tucker, R. D. (1986). Geology of the Hemne-Orkanger area, south-central Norway. *Norges Geologiske Undersøkelse Bulletin*, *404*, 1–24.

Tucker, R. D., Robinson, P., Solli, A., Gee, D. G., Thorsnes, T., Krogh, T. E., et al. (2004). Thrusting and extension in the Scandian hinterland, Norway: New U-Pb ages and tectonostratigraphic evidence. *American Journal of Science*, *304*, 477–532.

van Roermund, H. L. M. (2009). Recent progress in Scandian ultrahigh-pressure metamorphism in the northernmost domain of the Western Gneiss Complex, SW Norway: Continental subduction down to 180–200 km depth. *Journal of the Geological Society of London*, *166*(4), 739–751.

van Roermund, H. L. M., Carswell, D. A., Drury, M. R., & Heijboer, T. C. (2002). Microdiamonds in a megacrystic garnet websterite pod from Bardane on the island of Fjørtoft, western Norway: Evidence for diamond formation in mantle rocks during deep continental subduction. *Geology*, *30*(11), 959–962.

van Roermund, H. L. M., & Drury, M. R. (1998). Ultra-high pressure (P>6GPa) garnet peridotites in Western Norway: Exhumation of mantle rocks from > 185 km depth. *Terra Nova*, *10*, 295–301.

Vrijmoed, J. C., Smith, D. C., & van Roermund, H. L. M. (2008). Raman confirmation of microdiamond in the Svartberget Fe-Ti type garnet peridotite, Western Gneiss Region, Western Norway. *Terra Nova*, *20*, 295–301.

Vrijmoed, J. C., van Roermund, H. L. M., & Davies, G. (2006). Evidence for diamondgrade UHP metamorphism and fluid interaction in the Svartberget Fe-Ti garnet peridotite/websterite body, Western Gneiss Region, Norway. *Mineralogy and Petrology*, *88*, 381–405.

Vrijmoed, J. C., Podladchikov, Y. Y., Andersen, T. B., Hartz, E. H. (2009). An alternative model for ultra-high pressure in the Svartberget Fe-Ti garnet-peridotite, Western Gneiss Region, Norway. *European Journal of Mineralogy*, *21*(6), 1119–1133.

Wain, A. (1997). New evidence for coesite in eclogite and gneisses: Defining an ultrahigh-pressure province in the Western Gneiss region of Norway. *Geology*, *25*(10), 927–930.

Wain, A., Waters, D. J., Jephcoat, A., & Olijynk, H. (2000). The high-pressure to ultrahigh-pressure eclogite transition in the Western Gneiss Region, Norway. *European Journal of Mineralogy*, *12*(3), 667–687.

Walsh, E. O., Hacker, B. R., Grove, M., Gans, P. B., & Gehrels, G. (2007). Timing the exhumation of (ultra)high-pressure rocks across the Western Gneiss Region, Norway. *Geological Society of America Bulletin*, *119*(3–4), 289–301.